Gravitational waves from coalescing binaries and Doppler experiments

Bruno Bertotti

Dipartimento di Fisica Nucleare e Teorica, Università di Pavia
27100 Pavia, Italy

Alberto Vecchio

Max Planck Institut für Gravitationsphysik, Albert Einstein Institut
14473 Potsdam, Germany

Luciano Iess

Dipartimento di Ingegneria Aerospaziale, Università "La Sapienza"
00158 Roma, Italy
(February 7, 2008)

Abstract

Doppler tracking of interplanetary spacecraft provides the only method presently available for broad-band searches of low frequency gravitational waves ($\sim 10^{-5} - 1\,\mathrm{Hz}$). The instruments have a peak sensitivity around the reciprocal of the round-trip light-time T ($\sim 10^3 - 10^4$ sec) of the radio link connecting the Earth to the space-probe and therefore are particularly suitable to search for coalescing binaries containing massive black holes in galactic nuclei. A number of Doppler experiments – the most recent involving the probes ULYSSES, GALILEO and MARS OBSERVER – have been carried out so far; moreover, in 2002-2004 the CASSINI spacecraft will perform three 40 days data acquisition runs with expected sensitivity about twenty times better than that achieved so far.

Central aims of this paper are: (i) to explore, as a function of the relevant instrumental and astrophysical parameters, the Doppler output produced by *in-spiral* signals – sinusoids of increasing frequency and amplitude (the so-called *chirp*); (ii) to identify the most important parameter regions where to concentrate intense and dedicated data analysis; (iii) to analyze the all-sky and all-frequency sensitivity of the CASSINI's experiments, with particular emphasis on possible astrophysical targets, such as our Galactic Centre and the Virgo Cluster.

We consider first an ideal situation in which the spectrum of the noise is white and there are no cutoffs in the instrumental band; we can define

an *ideal* signal-to-noise ratio (SNR) which depends in a simple way on the fundamental parameters of the source – *chirp mass* $\mathcal{M}$ and luminosity distance – and the experiment – round-trip light-time and noise spectral level. For any *real* experiment we define the *sensitivity function* Υ as the degradation of the SNR with respect to its ideal value due to a coloured spectrum, the experiment finite duration T_1, the accessible frequency band (f_b, f_e) of the signal and the source's location in the sky. We show that the actual value of Υ crucially depends on the overlap of the band (f_b, f_e) with the instrument response: the sensitivity is best when $f_b \lesssim 1/T$ and f_e coincides with the frequency corresponding to the beginning of the merging phase. Furthermore, for any f_b and T_1, there is an optimal value of the chirp mass – the *critical chirp mass* $\mathcal{M}_c \propto f_b^{-8/5} T_1^{-3/5}$ – that produces the largest sensitivity function; lower values of $\mathcal{M}$ correspond to a smaller bandwidth and less SNR. Also the optimal source's location in the sky strongly depends on (f_b, f_e).

We show that the largest distance at which a source is detectable with CASSINI's experiments is ~ 600 Mpc and is attained for massive black holes of comparable masses $\sim 10^7 \, M_\odot$ and $f_b \sim 10^{-5}$ Hz. Sources not far from coalescence in the Virgo cluster with $10^6 \, M_\odot \lesssim \mathcal{M} \lesssim 10^9 \, M_\odot$ would be detectable with a SNR $\sim 1 - 30$. The SNR and the range of accessible masses reduce drastically when a smaller mass ratio is considered. We then turn the attention to galactic observations, in particular on the detectability of a coalescing binary in the Galactic Centre, where a small black hole of mass M_2 could be orbiting around the central massive one $M_1 \simeq 2 \times 10^6 \, M_\odot$. CASSINI would be able to pick up such systems with $M_2 \gtrsim 50 \, M_\odot$; for $M_2 \gtrsim 10^3 \, M_\odot$ the SNR could be as high as $\sim 100 - 1000$. It may also be possible to detect such binaries in more than one of the three CASSINI experiments, thus re-enforcing the confidence of detection.

Typeset using REVTEX

I. INTRODUCTION

The search for gravitational waves has greatly grown in the last few years: four ground based laser interferometers – LIGO [1], VIRGO [2], GEO600 [3] and TAMA [4] – with optimal sensitivity in the band $\sim 10\,\mathrm{Hz} - 1\,\mathrm{kHz}$ are now under construction and are scheduled to be in operation by the turn of the century; at the same time, the sensitivity of acoustic narrow-band devices in the kHz regime is steadily improving [5–9]. In this high frequency band the most interesting sources are connected to collapsed objects with mass in the range $\sim 1-1000\,M_\odot$. However, at low frequencies (below a few Hz) detectors on Earth are severely impaired by the seismic noise. To observe sources of higher mass one must use instruments in space, sensitive in the mHz band.

The Doppler tracking of interplanetary spacecraft [10] is the only method presently available to search for gravitational waves in the low frequency regime ($\sim 10^{-5} - 1\,\mathrm{Hz}$). Several experiments have been carried out so far, all of them with *non dedicated* space-probes: VOYAGER 1 [11], PIONEER 10 and 11 [12,13], ULYSSES [14,15], GALILEO and MARS-OBSERVER [16]. They suffer from the limitations of instrumentation designed for other purposes and from several disturbances, including those due to the ground sector; however, their sensitivity is astrophysically interesting, even though the rate of detectable events is uncertain and probably low, given the current instrument performances. At present a large amount of data is available: a major experiment lasted 28 days was carried out with ULYSSES in February/March 1992 [15] and a 20 days coincidence experiment was performed in the Spring 1993 with the spacecraft GALILEO, MARS-OBSERVER and ULYSSES [16] (see Table I).

The space-probe CASSINI – a NASA/ESA/ASI joint mission [17] – represents the next step in Doppler experiments: launched on October 15th 1997 with primary target the study of the Saturn system, the spacecraft carries on board much improved instrumentation and will perform three long (40 days each) data acquisition runs in 2002, 2003 and 2004 to search for gravitational waves [18] with expected sensitivity about twenty times better than that achieved so far. The next far away and much more ambitious projects will probably involve interferometers in space with arms of millions of km [19,20] (see also [21] and references therein for a review on detectors in space).

In the low frequency band we expect five main types of sources (for an extensive discussion regarding the whole gravitational wave spectrum we refer the reader to [22,23]):

1. Catastrophic, wide-band collapses of large masses, possibly in dense concentrations of matter and stars, leading to the formation of a massive black hole (MBH); the search for such signals motivated the original proposal of Doppler experiments [24].

2. Short-period binary systems of solar mass compact objects [25–27]; among them the binary pulsar PSR 1913+16 [28,29], whose study over the past 25 years has provided the most clear *indirect evidence* of the existence of gravitational waves [30]; however, stellar mass binaries are not detectable with present and near-future Doppler experiments, due to inadequate sensitivity and short duration.

3. Solar mass compact objects orbiting a massive black hole in galactic cores [31–33].

4. Binary systems of massive black holes spiraling together toward their final coalescence [34–36].

5. Backgrounds of gravitational waves of primordial origin or generated by the superposition of radiation coming from unresolved binaries [37–41].

Here we will consider signals emitted by binary systems containing massive black holes (MBH's), therefore sources at point 3 and 4, and the main goals of the paper are the exploration of the structure of the Doppler output produced by in-spiral signals from coalescing binaries and the analysis of the all-sky/all-frequency sensitivity of Doppler experiments with emphasis on the CASSINI mission.

Compelling arguments suggest the presence of MBH's in the nuclei of most galaxies, as the near-inevitable byproduct of the infall of gas in their potential well [42–44] and MBH's are invoked to explain a number of phenomena, such as the activity of quasars and active galactic nuclei [45–48]. However, the observational evidences of their existence come mainly from observations of relatively nearby galaxies, whose nuclei do not show significant activity. Central dark masses – that are believed to be "dead quasars" [49] – are mainly inferred by studying the spatial distribution and velocity of gas and/or stars in galactic cores. About ten candidate massive black holes, with mass in the range $\sim 10^6 - 10^9 \, M_\odot$, are known today and we refer the reader to [50–53] for recent reviews. The most striking evidences come from the mapping of the gas motion via the 1.35 cm water maser emission line in NCG 4258 and the observations in the near infrared band of the star motion in Our Galactic Centre. In the case of NCG 4258, observations with the Very Long Baseline Array have allowed to measure the velocity of the gas in the disk with an accuracy of 1 km/sec: the disc rotates with a velocity exactly in agreement with Kepler low, due to the presence of an obscure object of mass $\simeq 3.6 \times 10^6 \, M_\odot$ [54]. Regarding Our Galactic Centre, recent observations with the New Technology Telescope of the proper motion of stars in the core have shown that their speed scales as the inverse of the square root of the distance from the center up to 20000 km/sec; the inferred mass of the dark body is $\simeq 2.5 \times 10^6 \, M_\odot$ [55]. In both cases only exotic (and highly implausible) alternatives to a MBH can still be considered [56,57].

Many galaxies have experienced at least a merger since the epoch $z > 2$ [58,59]. If a MBH is present in each core of both interacting galaxies, the two massive objects would fall into the common potential well, forming a pair which losses energy and angular momentum through dynamical friction; eventually a binary forms and driven by radiation reaction precedes toward the final coalescence. This scenario provides, therefore, a quite natural way of producing massive binary black holes (MBHB's) [34]. The apparent precession and bending of jets in active galaxies [34,60] and Doppler shifted broad emission line peaks in quasars [61] are possible indirect evidences of the existence of such systems. Moreover observations of MBHB's in the nuclei 1928+738 [62], OJ287 [63,64] and 3C 390.3 [65] have been claimed.

MBH's in the center of galaxies are surrounded by a dense cluster of ordinary stars, whose tidal disruption provides the gas to refuel the central object, white dwarfs, neutron stars and low mass back holes, probably in the mass range $\sim 5 - 100 \, M_\odot$. Unless ordinary stars, compact objects are not disrupted by the hole and can occasionally be captured, presumably on highly eccentric orbits, forming binary systems with life shorter than the Hubble time.

Moreover the orbits of objects with mass $\gtrsim 5M_\odot$ around the central massive body would not be perturbed by other stars in the core providing therefore clean gravitational wave signals, that can be used to extract valuable information about the central object [66,67].

Taking the data analysis point of view, where the structure of the signal determines the choice of the optimal algorithm, it is convenient to divide the entire process of binary *coalescence* in three separate phases:

(a) *Adiabatic in-spiral*: the bodies are driven by radiation reaction from their initial distance to smaller separations, losing energy and angular momentum. The emitted gravitational wave corresponds to a sinusoid of increasing frequency and amplitude (the so-called *chirp*). In this paper we will make two important assumptions: (i) when the signal enters the sensitivity window of the detector, the orbit has already been circularized; in fact, the eccentricity e diminishes with the frequency f according to $e^2(t) \propto f^{-19/9}(t)$ [68]. A binary born with a period of 100 years, say, even with $e \sim 1$ would carry a residual eccentricity $\lesssim 10^{-4}$ when the signal can be picked up by the instrument. For binaries composed of two MBH's, that have undergone a common evolution inside a galactic core, this assumption is reasonable, even-though the full understanding of massive binary evolution before radiation reaction takes over still lacks [69–71]. The condition $e \ll 1$ is likely to be violated for solar mass compact objects orbiting a massive one, where the secondary body is captured in a highly elliptic orbit, which maintains a not negligible eccentricity throughout the in-spiral [31]. This would bring about a different scenario, with shorter life-time and emission of gravitational waves at multiples of the orbital frequency [72]. (ii) In the modelling of the waveform we will use the lowest-order Newtonian quadrupolar approximation, as we are mainly aiming at the estimation of the signal-to-noise ratio (SNR) and not at the construction of signal templates for matching filters [73,74].

(b) *Merger*: when the body separation r reaches a value of about $6\,M$, where M is the source's total mass, the orbit becomes unstable and the binary begins the final deadly phase of plunge-in. The signal consists in a wide-band burst of duration $\sim M$, but the details of the emitted radiation are in large part still unknown.

(c) *Ring-down*: the single black hole formed during the merging phase settles down oscillating according to quasi-normal modes. The emitted waves consist of a superposition of exponentially damped sinusoids.

In this paper we will concentrate on radiation emitted during the in-spiral phase. Such signals can be usefully classified according to the best algorithm to extract them in a given data set [15]:

I. *Periodic signals*: the rate of change of the frequency is too small to be detected with the instrumental frequency resolution. Here the ordinary techniques for the search of periodic oscillations of unknown frequency apply.

II. *Linearly "chirped" signals*: the frequency drift is larger than the frequency resolution of the detector but the change in frequency due to its second time derivative during the observation time can be neglected, so that we can assume a linear increase of $f(t)$ with a constant rate $\beta = df/dt$. An efficient technique to search for these signals has been developed in [75–77] and already applied to several data sets [15]; for every allowed β, the chirping signal is reduced to a periodic one and standard methods can be applied.

These two classes correspond to sources which are far from coalescence – in fact $df(t)/dt \propto f^{-8/3}(t)$, see Eq. (2.2) – and, for a given distance, weaker; therefore, the search depth (the maximum distance at which a binary would be detectable) is very limited: in [15] we showed that, with signals of this class, the Galactic Centre is marginally accessible with the best data available today.

III. *General chirps*: the assumed signal has the correct evolution in frequency, but the merger does not occur inside the record.

IV. *Chirps and bursts*: the record contains the final part of the chirping waveform, and the wide-band burst produced just before the engulfment of one black hole into the horizon of the other.

These classes of signals can be distinguished in the record by the frequency and its change; for a given frequency, its drift increases with the class. Roughly speaking, this ordering corresponds to stronger sources and, therefore, to larger attainable distances.

Although in the final phase of the in-spiral the two bodies have high velocities ($v/c > 0.1$) and the description of their gravitational wave emission requires a relativistic approach [22] we shall use the quadrupole Newtonian approximation for the estimation of the signal-to-noise ratio (SNR). The use of this approximation has the advantage that the in-spiral signal depends on only *one physical parameter*, the *chirp mass* $\mathcal{M}$, see Eq. (2.3). In principle it can be derived from the measurement of the frequency f and its rate of change df/dt; then the amplitude $A \propto \mathcal{M}^{5/3} f^{2/3}/D$ provides the distance D of the source. We can therefore determine, for any given experiment, the largest attainable distance; we call it, for a given class, the *ken* of the experiment. This is another example, similar to the one pointed out by Schutz in [78], of the power of gravitational wave astronomy when a simple source model is available. Central aim of the paper is to fully develop the richness of these concepts when applied to Doppler experiments and to link possible astrophysical sources (like those in the Virgo cluster and/or in the Galactic Centre) to the actual data. In particular we will apply the main results to the set of experiments scheduled during the CASSINI's mission.

Doppler tracking of interplanetary spacecraft provides a wide band detector of gravitational waves in the low frequency regime (but it can also be used as narrow-band xylophone instrument [79]). A very stable electromagnetic signal in the GHz radio band is continuously transmitted from the Earth to the spacecraft and coherently transponded back in order to monitor the change of their relative velocity. The optimal sensitivity of the detector is at frequencies of the order of the inverse of the round-trip light-time T of the Earth-spacecraft radio link. However, since in practice the duration of the experiment is not large, only a limited frequency interval of a chirping signal is accessible. There are two modes of search for a signal: if the frequency interval is small, *narrow band search*, one looks for sources far from the final plunge-in, hence at a small distance. In a *wide band search* the signal is stronger and one can detect radiation emitted by binary systems further away. In the past, the analysis of Doppler data has been confined mainly to the narrow band case (classes I and II); in this paper we concentrate on the more interesting wide band case and aim at sources at larger distances, but detectable only for a smaller fraction of their lifetime. The largest "ken" is, of course, attained for class IV, which merges into the class of generic, wide-band

bursts. The search for bursts in the records of the 1993 GALILEO-MARS OBSERVER-ULYSSES coincidence experiment is currently in progress [16]. However this analysis must be a rough one, as the structure of the signal in this strongly relativistic regime is essentially unknown and the use of data collected in coincidence by several instruments is crucial.

The the paper is organized as follows. In Sec. II we review the basic concepts and formula (partially to fix notation) regarding the gravitational wave emission from binaries. In Sec. III we introduce the signal $y(t)$ produced at the output of a Doppler detector by a gravitational wave train $h(t)$: in the Fourier space, $\tilde{y}(f)$ is the product of $\tilde{h}(f)$ and the Doppler *three-pulse response function* $\tilde{r}_\theta(f)$; we review the main properties of $\tilde{r}_\theta(f)$ and in particular we stress its different structure in the low ($f \lesssim 1/T$) and high ($f \gtrsim 1/T$) frequency regimes. Sec. IV contains the main results of the paper: a thorough analysis of the signal-to-noise ratio produced by in-spiral signals in Doppler experiments as a function of the parameters that characterize the source and the instrument: the chirp mass $\mathcal{M}$ (and the mass ratio), the instantaneous emission frequency of the signal f_b when the instrument is "turned on", the duration of the observation T_1, the structure of the instrument noise spectral density $S_n(f)$, the location θ of the source in the sky with respect to the detector arm and the round-trip light-time T. This analysis is carried out in full generality and can be applied to any Doppler experiment. We define the *ideal* SNR, ρ_{id}, as that corresponding to unlimited bandwidth, $\theta = \pi/2$ and flat noise spectrum: ρ_{id} depends only on $\mathcal{M}$, T, D and the noise spectral level S_0. Of course, in a real experiment several factors – among which the finite observation time, the signal bandwidth, the frequency-dependent noise spectral density and the position of the source in the sky – contribute to degrade the SNR. Indeed, we define the *sensitivity function* Υ as the actual SNR with respect to its ideal value. Υ is extensively studied in Sec. IV A. In particular we show that the maximum value of Υ is achieved when $0.1/T \lesssim f_b \lesssim 1/T$ and the binary chirp mass is close to what we call its critical value $\mathcal{M}_c \propto T_1^{-3/5} f_b^{-8/5}$. In Sec. IV B we study the CASSINI's sensitivity (and compare it with that of ULYSSES), with emphasis on possible sources in the Virgo Cluster and the Galactic Center. We show that the maximum reachable distance is ~ 600 Mpc; binaries close to the final coalescence with $10^6 \, M_\odot \lesssim \mathcal{M} \lesssim 10^9 \, M_\odot$ and comparable masses would be detectable in the Virgo cluster with SNR up to 30; in galactic searches, CASSINI would be able to pick up (possibly in all three data sets) signals from the in-spiral of a secondary black hole of mass $M_2 \gtrsim 50 \, M_\odot$ onto the central one $M_1 \simeq 2 \times 10^6 \, M_\odot$. Finally, Sec. V contains a discussion about the probability of success of Doppler experiments based on simple conventional astrophysical scenarios and our conclusions.

We take units in which $c = G = 1$, so that velocities are dimensionless and $10^6 \, M_\odot \simeq 4.926 \, \mathrm{sec}$.

II. THE EXPECTED SIGNAL

A. The chirped precursor

We consider a binary system of two compact objects of mass M_1 and M_2; $M \equiv M_1 + M_2$ and $\mu \equiv M_1 M_2/M$ are the total and reduced mass, respectively; the orbital parameters

evolve secularly due to the loss of energy and angular momentum by emission of gravitational waves.

We shall assume that, when the gravitational signal enters the sensitivity window of the detector, the radiation reaction has already circularized the orbit. Under this assumption, in the Newtonian quadrupolar approximation, the frequency f of the emitted gravitational wave is twice the orbital frequency of the binary, namely

$$f^2(t) = \frac{M}{\pi^2 r^3(t)} , \tag{2.1}$$

where $r(t)$ is the orbital separation. In the Newtonian model, $f(t)$ evolves according to [80]

$$\dot{f}(t) = \frac{96}{5} \pi^{8/3} \mathcal{M}^{5/3} f^{11/3}(t) , \tag{2.2}$$

where the dot indicates the time derivative and

$$\mathcal{M} \equiv \mu^{3/5} M^{2/5} = \eta^{3/5} M \qquad \left(\eta \equiv \frac{\mu}{M} \leq 1/4 \right) \tag{2.3}$$

is the so-called *chirp mass*; in this approximation $\mathcal{M}$ is the only *dynamical* parameter that regulates the evolution of the frequency and the amplitude of the wave.

Let us consider a signal emitted by a binary at a luminosity distance D and let ι be the angle between the wave propagation direction and the orbital angular momentum $\boldsymbol{L}$. The strain at the detector reads

$$\begin{aligned} h(t) &= h_+(t) \cos 2\varphi + h_\times(t) \sin 2\varphi \\ &= A(t) \cos \left[2\pi \int^t dt' f(t') + \varphi_0 \right] , \end{aligned} \tag{2.4}$$

where $h_+(t)$ and $h_\times(t)$ are the two independent polarization states [90], and φ a polarization angle;

$$\begin{aligned} A(t) &= 2 \, Q(\iota, \varphi) \frac{\mathcal{M}^{5/3}}{D} [\pi f(t)]^{2/3} \\ &= 1.3 \times 10^{-15} \, Q(\iota, \varphi) \left(\frac{D}{\mathrm{Mpc}} \right)^{-1} \left(\frac{f}{10^{-4}\mathrm{Hz}} \right)^{2/3} \left(\frac{\mathcal{M}}{10^6 M_\odot} \right)^{5/3} , \end{aligned} \tag{2.5}$$

is the amplitude of the signal and

$$\varphi_0 = \tan^{-1} \left[\frac{2 \cos \iota \sin(2\varphi)}{\cos(2\varphi)(1 + \cos^2 \iota)} \right] \tag{2.6}$$

gives the polarization phase. The quantity

$$Q^2(\iota, \varphi) = [\cos^2(2\varphi)(1 + \cos^2 \iota)^2 + 4 \cos^2 \iota \sin^2(2\varphi)] \tag{2.7}$$

depends on the orientation of the binary and, for random values, $\langle Q^2 \rangle = 8/5$, where $\langle \rangle$ stands for the average with respect to ι and φ: $Q(\iota, \varphi)$ ranges from 0 (for $\iota = \pi/2, \varphi = \pi/4$) to 2 (for $\iota = 0$ or π) [91].

8

Integrating Eq. (2.2), it is straightforward to derive the frequency evolution of the wave:

$$f(t) = \frac{1}{8\pi} \left(\frac{5}{t_n}\right)^{3/8} \mathcal{M}^{-5/8} \left(1 - \frac{t}{t_n}\right)^{-3/8} , \tag{2.8}$$

and therefore the phase of the gravitational signal reads

$$\Phi(t) = 2\pi \int_t^{t_n} dt' f(t') = \Phi_n - 2\left(\frac{t_n - t}{5\mathcal{M}}\right)^{5/8} ; \tag{2.9}$$

equivalently,

$$t(f) = t_n - 5(8\pi f)^{-8/3}\mathcal{M}^{-5/3} , \tag{2.10}$$

$$\Phi(f) = \Phi_n - 2(8\pi\mathcal{M}f)^{-5/3} . \tag{2.11}$$

From Eq. (2.2), one can also derive the number of Newtonian wave cycles spent by a binary while it sweeps the relevant frequency interval

$$\mathcal{N}(f) = \int_f^\infty \frac{f'}{\dot{f}'} df' = \mathcal{N}_n - \frac{1}{\pi}(8\pi\mathcal{M}f)^{-5/3} . \tag{2.12}$$

t_n, Φ_n and $\mathcal{N}_n$ are integration constants, defined as the values that $t(f)$, $\Phi(f)$ and $\mathcal{N}(f)$ formally take when $f = \infty$ ($r = 0$). Of course, the signal must be cut off when the in-spiral phase ends and the merger begins. The fully relativistic two-body problem is still unsolved; it is mainly investigated using post-Newtonian approximations (see [81,82] and references therein) and numerical techniques (see [94–96] and references therein). For simplicity we will neglect the radiation coming from frequencies higher than

$$f_{\text{isco}} = \frac{1}{6^{3/2}\pi M} \simeq 1.9 \times 10^{-3} (4\eta)^{3/5} \left(\frac{\mathcal{M}}{10^6 M_\odot}\right)^{-1} \text{Hz} , \tag{2.13}$$

corresponding to the *innermost stable circular orbit* $r_{\text{isco}} = 6M$ for a test mass in the Schwarzschild field of a mass M. For $r < r_{\text{isco}}$ (and velocity larger than $v_{\text{isco}} \simeq 0.408$) orbits are unstable. For general black holes and mass ratios we can write $r_{\text{isco}} = 6kM$, with $k \approx 1$ (several methods have been used to estimate the exact value of k, but a satisfactory answer still lacks; see [97–100] for further details). In the Newtonian approximation we assume that $f_{\text{isco}} = f(t_c)$ separates, at the time t_c, the in-spiral phase from the broad band plunge-in. The major feature of the relativistic corrections is, therefore, to *anticipate* the final plunge.

If an experiment takes place in the time interval from $t = 0$ to $t = T_1$, we define

$$f_b \equiv f(t = 0) \tag{2.14}$$

as the frequency at which the signal enters the record at $t = 0$; the frequency at the end, after the observation time T_1, is

$$f_e \equiv f(t = T_1) = \min\left[f_b\left(1 - \frac{T_1}{t_n}\right)^{-3/8}, f_{\text{isco}}\right] . \tag{2.15}$$

9

If $f_b(1 - T_1/t_n)^{-3/8} > f_{\text{isco}}$ the record includes the merger signal and is of class IV; otherwise we have class III signals. The Newtonian time to coalescence for a system radiating at frequency f_b at the beginning of the record is given by:

$$\tau_n = 5 \, (8\pi f_b)^{-8/3} \, \mathcal{M}^{-5/3} \, . \tag{2.16}$$

It is also useful to note that the time for a signal to sweep from the frequency f_b to the beginning of the final coalescence, that we suppose to occur at $f = f_{\text{isco}}$, is

$$\tau_c = 5 \, (8\pi)^{-8/3} \, \mathcal{M}^{-5/3} \, \left(f_b^{-8/3} - f_{\text{isco}}^{-8/3} \right) \, . \tag{2.17}$$

We define

$$f_B \equiv f_{\text{isco}} \left(1 + \frac{T_1}{5(8\pi f_{\text{isco}})^{-8/3} \, \mathcal{M}^{-5/3}} \right)^{-3/8} \tag{2.18}$$

as the initial frequency of a gravitational wave whose final frequency is f_{isco}; it depends on $\mathcal{M}$, η and T_1 and corresponds to the largest initial frequency that produces class III signals.

On the base of the model of the waveform we can now formalize the distinction of the signals in classes that we have introduced in Sec. I. Being based upon the actual record, it is particularly useful for data analysis. It refers to the frequency resolution $1/T_1$ of the experiment and will allow us to divide the two-dimensional parameter space $(\mathcal{M}, f_b)$, where the in-spiral signal is defined, into a *periodic region*, a *linear region* and a *general chirp region* (of class III and IV, depending whether the final burst is within the record or not). This distinction is justified by the great simplicity and low computational load of the data analysis when the frequency is constant (class I) or varies linearly with time (class II); these two cases are extensively discussed, and applied to the data of ULYSSES' second opposition, in [15]. When

$$T_1^2 \dot{f}(t) = \frac{96}{5} \pi^{8/3} T_1^2 \mathcal{M}^{5/3} f^{11/3} < 1 \qquad \text{(class I)} \tag{2.19}$$

we have periodic signals; when

$$T_1^3 \frac{\ddot{f}(t)}{2} = \frac{16896}{25} \pi^{16/3} T_1^3 \, \mathcal{M}^{10/3} f^{19/3} < 1 \qquad \text{and} \qquad T_1^2 \dot{f}(t) > 1 \qquad \text{(class II)} \tag{2.20}$$

linear signals;

$$\frac{T_1^3 \ddot{f}(t)}{2} > 1 \qquad \text{and} \qquad f_b < f_{\text{isco}} \qquad \text{(class III/IV)} \tag{2.21}$$

correspond to general chirps [101]. Referring to a chirp mass $\mathcal{M}$ and observation time T_1, the initial frequency f_b that separates out the four regimes reads:

$$f_b \simeq \begin{cases} 5.1 \times 10^{-5} \left(\frac{T_1}{10^6 \, \text{sec}} \right)^{-6/11} \left(\frac{\mathcal{M}}{10^6 \, M_\odot} \right)^{-5/11} \text{Hz} & (I - II) \\[2ex] 5.4 \times 10^{-5} \left(\frac{T_1}{10^6 \, \text{sec}} \right)^{-9/19} \left(\frac{\mathcal{M}}{10^6 \, M_\odot} \right)^{-10/19} \text{Hz} & (II - III) \\[2ex] 1.9 \times 10^{-3} \, (4\eta)^{3/5} \left(\frac{\mathcal{M}}{10^6 \, M_\odot} \right)^{-1} \left[1 + 8.7 \times 10^2 \, (4\eta)^{8/5} \left(\frac{T_1}{10^6 \, \text{sec}} \right) \left(\frac{\mathcal{M}}{10^6 \, M_\odot} \right)^{-1} \right]^{-8/3} \text{Hz} & (III - IV) \end{cases} \tag{2.2}$$

The partition of the plane $(\mathcal{M}, f_b)$ in classes for a single CASSINI's experiment ($T_1 = 40$ days) is given in Fig. 1. The values of τ_n that correspond to the transition between two adjacent classes read

$$
\tau_n \simeq \begin{cases} 6.1 \times 10^7 \left(\frac{\mathcal{M}}{10^6\, M_\odot}\right)^{-5/11} \left(\frac{T_1}{10^6 \mathrm{sec}}\right)^{16/11} \mathrm{sec} & (I - II) \\ 2.6 \times 10^6 \left(\frac{\mathcal{M}}{10^6\, M_\odot}\right)^{-5/19} \left(\frac{T_1}{10^6 \mathrm{sec}}\right)^{24/19} \mathrm{sec} & (II - III) \\ 1.1 \times 10^3 \left(\frac{\eta}{1/4}\right)^{-8/5} \left(\frac{\mathcal{M}}{10^6\, M_\odot}\right) \mathrm{sec} & (III - IV) \end{cases} \tag{2.23}
$$

As we have mentioned in the Introduction, class I to IV correspond to gravitational wave emission increasingly closer to the final merger and, therefore, to stronger signals. In Fig. 2 we show the frequency f_b and the characteristic time τ_n that separate the four classes as function of the observation time. For typical present and future data sets (see Table I) and reasonable sources, most signals would show up in class III or IV.

We introduce now the Fourier transform $\tilde{h}(f)$ of the real function $h(t)$:

$$
\tilde{h}(f) = \int_{-\infty}^{\infty} e^{-2\pi i f t} h(t)\, dt = \tilde{h}^*(-f) \tag{2.24}
$$

and hereafter we will work in the more convenient Fourier space. When the frequency $f(t)$ and the amplitude $A(t)$ (Eqs. (2.2) and (2.5)) vary over a time scale much longer than $1/f(t)$ it is convenient to use the *stationary phase approximation* in order to compute the integral (2.24). In our case

$$
\frac{1}{f(t)} \frac{d}{dt} \ln[A(t)] \propto \frac{1}{f(t)} \frac{d}{dt} \ln[f(t)] \propto [\mathcal{M} f(t)]^{5/3}\,, \tag{2.25}
$$

where we have neglected numerical coefficients of proportionality. The evaluation of the actual error involved in this approximation is a delicate matter; however, in the limit

$$
[\mathcal{M} f(t)]^{5/3} \ll 1\,, \tag{2.26}
$$

we expect this approximation to be satisfactory for the assessment of the signal-to-noise ratio. Note also that

$$
[\mathcal{M} f(t)]^{5/3} < (\mathcal{M} f_{\mathrm{isco}})^{5/3} \propto \left(\frac{\mathcal{M}}{M}\right)^{5/3} \propto \eta\,, \tag{2.27}
$$

so that the limit (2.26) is formally fulfilled for a small mass ratio. Of course, as usual, the approximation will be fearlessly pushed to the limits of validity.

In the stationary phase approximation to the integral (2.24), for a frequency f only a small interval δt contributes around the time $t(f)$ where

$$
f(t) = f\,. \tag{2.28}
$$

Note the slight inconsistency of notation: f is now the independent variable in the Fourier space, while earlier we have introduced $f(t)$ as a function of time. The time interval is of order

$$\delta t = [\dot{f}(t)]^{-1/2} = \left(\frac{5}{96}\right)^{1/2} \pi^{-4/3} \mathcal{M}^{-5/6} f^{-11/6}(t), \tag{2.29}$$

corresponding to a local bandwidth $\delta f = 1/\delta t$. A finite record in $(0, T_1)$ will pick up only the part of the spectrum between f_b and f_e; since dropping the data outside $(0, T_1)$ is equivalent to convolving with $\sin(f T_1)/f$, one wonders how this can kill the Fourier components outside (f_b, f_e). The answer is that outside the frequency range defined by $f = f(t)$, $(0 \le t \le T_1)$, the phase of the Fourier integral (2.24) has fast oscillations. The Fourier amplitude is then of order

$$A \delta t \approx \frac{\mathcal{M}^{5/6}}{D} f^{-7/6}. \tag{2.30}$$

The full expression of the Fourier transform of $h(t)$, Eq. (2.4), computed according to the stationary phase approximation is [102]:

$$\tilde{h}(f) = \begin{cases} \mathcal{A} f^{-7/6} e^{i\Psi(f)} & f \le f_{\text{isco}} \\ 0 & f > f_{\text{isco}} \end{cases}, \tag{2.31}$$

where

$$\mathcal{A} = \left(\frac{5}{6}\right)^{1/2} \frac{1}{4\pi^{2/3}} Q(\iota, \phi) \frac{\mathcal{M}^{5/6}}{D} \tag{2.32}$$

is the amplitude and

$$\Psi(f) = 2\pi f t_n - \Phi_n - \frac{\pi}{4} + \frac{3}{4}(8\pi \mathcal{M} f)^{-5/3} \tag{2.33}$$

the phase.

The existence of an analytic expression of the in-spiral signal in the Fourier space justifies its use. As compared with the analysis in the time domain, it offers two main advantages: the instrumental response function, see Eqs. (3.1)–(3.4), is a simple multiplicative factor and we can easily deal with coloured noise (see Sections III and IV).

B. The final burst

The theoretical knowledge of the signal emitted during the merger of two black holes is at present quite poor. It involves the computation of the solutions of the Einstein equation in highly non linear regimes and this issue is currently tackled by several groups mainly by means of intensive numerical computation on state-of-the art machines (see [94–96] and references therein). Here we present a simple model for the energy spectral density dE/df emitted during the merger, following the approach presented in [103]; although quite naive and crude, it is reasonable for an order of magnitude comparison of the sensitivity of Doppler experiments to in-spiral and merger signals, which shall be carried out in Sec. IV.

The wave emitted during the final stages of the life of a binary system is spread over a wide band. For sake of simplicity, and lack of more detailed knowledge, we assume it to

12

be confined between the final frequency of the in-spiral, *i.e.* f_{isco}, and the characteristic frequency f_{qnm} at which the ring-down emission sets in. We will assume

$$f_{\mathrm{qnm}} \simeq \frac{1}{2\,\pi\,M} = 3.2 \times 10^{-2} \left(\frac{M}{10^6\,M_\odot}\right)^{-1} \mathrm{Hz} \qquad (2.34)$$

that roughly corresponds to the frequency of the quasi-normal oscillation for the $l = m = 2$ mode of a Kerr black hole with dimensionless spin parameter $\simeq 0.98$. This choice of f_{qnm} can be justified as follows: the $l = m = 2$ mode, very likely to be excited at the end of the black hole plunge-in, is that with the longest damping time and the resulting massive black hole will quite probably carry a large intrinsic angular momentum.

The total energy E_{merg} radiated during the merger phase, and confined into the frequency interval $(f_{\mathrm{isco}}, f_{\mathrm{qnm}})$, is proportional to μ^2/M [104] and can be written as

$$E_{\mathrm{merg}} = \epsilon_{\mathrm{merg}} \, F\left(\frac{\mu}{M}\right) M \,, \qquad (2.35)$$

where ϵ_{merg} denotes the efficiency of the process and $F(\mu/M) = (4\mu/M)^2$; of course, a precise estimate of ϵ_{merg} would require a full numerical calculation, but a reasonable order of magnitude guess yields $\epsilon_{\mathrm{merg}} \sim 0.1$ (see [103] and references therein). Lacking any evidence about the structure of the energy spectrum, we will make the simple assumption that E_{merg} is uniformly distributed over the band $(f_{\mathrm{qnm}}, f_{\mathrm{isco}})$, so that

$$\frac{dE_{\mathrm{merg}}}{df} = \begin{cases} \frac{E_{\mathrm{merg}}}{(f_{\mathrm{qnm}} - f_{\mathrm{isco}})} & f_{\mathrm{isco}} \leq f \leq f_{\mathrm{qnm}} \\ 0 & f < f_{\mathrm{isco}} \ \mathrm{and} \ f > f_{\mathrm{qnm}} \end{cases} . \qquad (2.36)$$

We recall here that the energy spectrum of the radiation emitted during the in-spiral phase is given by

$$\frac{dE_{\mathrm{insp}}}{df} = \begin{cases} \frac{\pi^{2/3}}{3}\,\mathcal{M}^{5/3}\,f^{-1/3} & f \leq f_{\mathrm{isco}} \\ 0 & f > f_{\mathrm{isco}} \end{cases} . \qquad (2.37)$$

Eqs. (2.36) and (2.37) will enable us to compare the detectability of coalescing binaries during the in-spiral and merger phase with Doppler experiments, as the optimal signal-to-noise ratio is simply related to dE/df, see Eq. (4.5); this analysis is carried out in Sec. IV.

III. DOPPLER RESPONSE TO IN-SPIRAL SIGNALS

In a Doppler experiment, the Earth and a spacecraft are used as the end-points of a gravitational wave detector [10]. A radio link is transmitted from the Earth to the spacecraft, coherently transponded and sent back to the Earth, where, at the time t, its frequency is measured with great accuracy; comparing the emitted and received frequency – ν_0 and $\nu(t)$, respectively – one determines the Doppler shift $(\nu(t) - \nu_0)/\nu_0$ as a function of time. The contribution to this effect produced by a gravitational wave $h(t)$ is usually called the *Doppler signal $s(t)$* and reads [10]

$$s(t) = \int_{-\infty}^{\infty} dt' r_\theta(t - t')h(t') \, ; \tag{3.1}$$

$$r_\theta(t) = \frac{\cos\theta - 1}{2}\delta(t) - \cos\theta \, \delta\left(t - \frac{\cos\theta + 1}{2}T\right) + \frac{1 + \cos\theta}{2}\delta(t - T) \tag{3.2}$$

is the characteristic *three-pulse response* of the instrument, as the incoming signal $h(t)$ is repeated in the detector output at three different times (and with different amplitude): t, $t - (\cos\theta + 1)T/2$ and $t - T$; $r_\theta(t)$ depends on the angle θ between the spacecraft and the source and the round-trip light-time $T = 2L$ out to the distance L of the probe. In the frequency domain the Doppler signal (3.1) takes a very simple form:

$$\tilde{s}(f) = \tilde{r}_\theta(f)\tilde{h}(f) \, , \tag{3.3}$$

where $\tilde{h}(f)$ is given by Eq. (2.31) and the Fourier transform of $r_\theta(t)$ reads

$$\tilde{r}_\theta(f) = \frac{\cos\theta - 1}{2} - \cos\theta \exp\left[\pi i(1 + \cos\theta)fT\right] + \frac{1 + \cos\theta}{2}\exp[2\pi i fT] \, . \tag{3.4}$$

Since the frequency f appears multiplied by the round-trip light-time T, we introduce the dimensionless variable

$$\xi \equiv fT \, . \tag{3.5}$$

In agreement with the Weak Equivalence Principle, the response of the instrument goes to zero in the low frequency limit $\xi \ll 1$ (this is the regime in which ground and space-based interferometers work):

$$\tilde{r}_\theta(\xi) = i\pi\xi \sin^2\theta - \frac{1}{2}\pi^2\xi^2 \sin^2\theta(2 + \cos\theta) + O(\xi^3) \, . \tag{3.6}$$

To lowest order the angle θ only affects the coefficient. As ξ increases, $\tilde{r}_\theta(\xi)$ develops modulations in amplitude and, more importantly, in phase, that depend on θ. The beats produced by the superposition of the signals at the times t, $t - (\cos\theta + 1)T/2$ and $t - T$ result in minima and maxima of the amplitude superimposed to the general increasing trend $A(t) \propto f^{2/3}(t)$, see Eq. (2.5), as shown in Fig 3; they strongly depend on the angle θ and provide a sensitive signature for its determination.

The transversal character of gravitational waves is reflected in the forward ($|\theta| \ll 1$) and backward ($|\theta'| = |\pi - \theta| \ll 1$) limits, when the wave travels in a direction almost parallel to the Earth-spacecraft line:

$$\tilde{r}_\theta(\xi) = \frac{\theta^2}{4}\left[(1 + 2\pi i\xi)e^{2\pi i\xi} - 1\right] + O(\theta^4) \qquad (|\theta| \ll 1) \, , \tag{3.7}$$

$$\tilde{r}_\theta(\xi) = \frac{\theta'^2}{4}\left[e^{2\pi i\xi} - 1 + 2\pi\xi\right] + O(\theta'^4) \qquad (|\theta'| = |\pi - \theta| \ll 1) \, ; \tag{3.8}$$

14

both tend to zero; they have the same limiting amplitude, but different phases. Note that the two limits are not uniform and are violated at high frequency ($\xi \gg 1$).

For generic values of θ it is convenient to use the squared modulus of (3.4):

$$
\begin{aligned}
|\tilde{r}_\theta(\xi)|^2 = {} & \frac{3\cos^2\theta + 1}{2} + \frac{\cos^2\theta - 1}{2}\cos(2\pi\xi) \\
& - \cos\theta(\cos\theta + 1)\cos[(\cos\theta - 1)\pi\xi] \\
& - \cos\theta(\cos\theta - 1)\cos[(\cos\theta + 1)\pi\xi]\,,
\end{aligned}
\tag{3.9}
$$

which, in the limit $\xi \ll 1$, reads

$$
|\tilde{r}_\theta(\xi)|^2 = \pi^2\xi^2\sin^4\theta\left[1 - \frac{1}{3}\left(1 - \frac{1}{4}\cos^2\theta\right)\pi^2\xi^2\right] + O(\xi^5)\,.
\tag{3.10}
$$

$|\tilde{r}_\theta(\xi)|^2$, which is shown in Fig 4, is an even function of $\cos\theta$, sum of four functions periodic in ξ, with frequencies 0, 1, $(1 - \cos\theta)/2$ and $(1 + \cos\theta)/2$, respectively. Its average is $(3\cos^2\theta + 1)/2$. As example, for $\theta \to \pi/2$ the response reads

$$
\begin{aligned}
|\tilde{r}_\theta(\xi)|^2 = {} & \sin^2(\pi\xi) + [(1 - \cos(\pi\xi))^2 \\
& - 2\pi\xi\sin(\pi\xi)](\theta - \frac{\pi}{2})^2 + O[(\theta - \frac{\pi}{2})^4]
\end{aligned}
\tag{3.11}
$$

and it has a maximum for $\xi = 1/3$. For large frequencies it develops more and more lobes with the angular scale $1/\xi$ (see Fig. 4). Averaging $|\tilde{r}_\theta(\xi)|^2$ over the direction θ one obtains the mean square response of the detector:

$$
\begin{aligned}
\overline{|\tilde{r}_\theta(\xi)|^2} & = \frac{1}{2}\int_{-1}^{1}|\tilde{r}_\theta(\xi)|^2\,d(\cos\theta) \\
& = \frac{\pi^2\xi^2 - 3}{\pi^2\xi^2} - \frac{\pi^2\xi^2 + 3}{3\pi^2\xi^2}\cos(2\pi\xi) + \frac{2}{\pi^3\xi^3}\sin(2\pi\xi)\,,
\end{aligned}
\tag{3.12}
$$

which, in the low and high frequency limit, reads:

$$
\overline{|\tilde{r}_\theta(\xi)|^2} = \begin{cases} \frac{8}{15}\pi^2\xi^2\left(1 - \frac{29}{84}\pi^2\xi^2\right) + O(\xi^6) & (\xi \ll 1) \\ 1 - \frac{1}{3}\cos(2\pi\xi) & (\xi \gg 1) \end{cases}\,.
\tag{3.13}
$$

During an experiment neither the angle θ nor the round-trip light-time T are exactly constant, mainly due to the motion of the Earth; their time-variation induces changes in the phase of the filter of order $\pi\Delta\theta\,fT$ and $\pi f\Delta T$. For the latter $\Delta T \approx 2\,v_\oplus T_1/c \approx 2 \times 10^{-4}T_1$ ($v_\oplus \simeq 30$ km/sec is the orbital velocity of the Earth) and the effect is relevant when

$$
2 \times 10^{-4}\pi fT_1 \approx 1\,,
\tag{3.14}
$$

while the angle θ affects the phase by a smaller amount. For CASSINI's experiments this occurs at about 5 mHz, which is above the most important sensitivity region of the instrument (see next Section). Indeed, we will consider constant both T and θ.

15

IV. SENSITIVITY OF DOPPLER EXPERIMENTS

The Fourier output of the detector

$$\tilde{y}(f) = \tilde{s}(f) + \tilde{n}(f) \tag{4.1}$$

is the sum of the signal $\tilde{s}(f)$ and the noise $\tilde{n}(f)$. The noise is assumed to be stationary, with zero mean and spectral power density

$$\langle \tilde{n}^*(f)\tilde{n}(f') \rangle = \delta(f - f')S_n(f) \,. \tag{4.2}$$

We consider single-sided noise spectra $S_n(f)$, formally from 0 to $+\infty$, and take into account the finite instrumental bandwidth with suitably large values at the boundaries of the sensitivity window. When $S_n(f)$ is white the corresponding *Allan deviation* [105]

$$\sigma_y = \sqrt{\frac{S_n}{\tau}} \tag{4.3}$$

is inversely proportional to the square root of the integration time τ; for coloured spectra, see, e.g., [106]. For simplicity we use a continuous spectrum $S_n(f)$, although, over an experiment of duration T_1 and with sampling time Δ_s, the spectrum consists of discrete Fourier modes spaced by $1/T_1$, from $1/T_1$ to the Nyquist frequency $1/(2\Delta_s)$.

Since the shape of the signal in the in-spiral phase can be accurately predicted, the technique of *matched filtering* is particularly suitable (see, e.g., [73,74] and references therein). It can be shown that if the signal $\tilde{s}(f)$ is known to within a constant (and real) amplitude h, its least square estimator has a variance given by

$$\left(\frac{s}{\sigma_n}\right)^2 = \rho^2 = 4 \int_0^\infty \frac{|\tilde{s}(f)|^2}{S_n(f)} \, df \,. \tag{4.4}$$

The quantity ρ is appropriately called the *signal-to-noise ratio* and is related to the energy spectrum of the radiation dE/df by the relation

$$\rho^2 \propto \frac{1}{D^2} \int_0^\infty \frac{|\tilde{r}_\theta(f)|^2}{f^2 \, S_n(f)} \frac{dE}{df} \, df \,. \tag{4.5}$$

It is useful to introduce an ideal reference value of the SNR and to discuss its dependence on the main parameters. From Eq. (3.13), we can approximate the instrumental filter r_θ, as follows:

$$|\tilde{r}_\theta(\xi)|^2 \sim \begin{cases} \xi^2 & (\xi < 1) \\ 1 & (\xi > 1) \end{cases} \,. \tag{4.6}$$

With a white noise spectrum $S_n = \sigma_y^2 \tau = $ const., and taking into account the frequency dependence of the signal (see Eqs. (2.31), (3.3) and (4.6)), we have

$$\frac{|\tilde{s}(f)|^2}{S_n(f)} \propto \begin{cases} \frac{\xi^{-1/3}}{\sigma_y^2 \tau} & (\xi < 1) \\ \frac{\xi^{-7/3}}{\sigma_y^2 \tau} & (\xi > 1) \end{cases} \,. \tag{4.7}$$

16

This is a decreasing function of ξ, both sides are integrable, so that in this ideal case the bulk of the sensitivity comes from $f \sim 1/T$ (cfr. also Fig 7). We can define the *ideal* SNR by taking $\xi_b \equiv f_b T \ll 1$, $\xi_e \equiv f_e T \gg 1$ and the direction angle $\theta = \pi/2$, for which $|\tilde{r}_{\pi/2}(\xi)|^2 = \sin^2(\pi\xi)$; from Eqs. (2.31), (2.32) and (4.4), averaging over the source angles ι, φ, we get

$$\rho_{\text{id}}^2 = K \frac{T^{4/3} \mathcal{M}^{5/3}}{\sigma_y^2 \tau D^2}, \tag{4.8}$$

where

$$K \equiv \frac{5}{24\pi^{4/3}} \frac{\langle Q^2(\iota, \varphi) \rangle}{T^{4/3}} \int_0^\infty f^{-7/3} |\tilde{r}_{\pi/2}(f)|^2 \, df$$
$$= \frac{2^{1/3} \pi}{3^{3/2} \Gamma(7/3)} \simeq 0.64. \tag{4.9}$$

The ideal *ken* – the largest distance at which a source is ideally detectable at $\rho_{\text{id}} = 1$ – is

$$D_{\text{id}} = K^{1/2} \frac{T^{2/3} \mathcal{M}^{5/6}}{\sigma_y \sqrt{\tau}}. \tag{4.10}$$

For the CASSINI's mission (see Table I), with $T = 10^4$ sec and $\sigma_y^2 \tau = 9 \times 10^{-26} \, \text{Hz}^{-1}$, it has the value

$$D_{\text{id}} \simeq 45 \left(\frac{\mathcal{M}}{10^6 M_\odot} \right)^{5/6} \left(\frac{T}{10^4 \text{sec}} \right)^{2/3} \left(\frac{\sigma_y^2 \tau}{9 \times 10^{-26} \, \text{Hz}^{-1}} \right)^{-1/2} \text{Mpc}. \tag{4.11}$$

For ULYSSES the the ideal ken for $\mathcal{M} = 10^6 M_\odot$, is $\simeq 3$ Mpc; in the coincidence experiment, the values for GALILEO and MARS-OBSERVER are $\simeq 0.5$ Mpc and $\simeq 2$ Mpc, respectively, where the values of σ_y, τ and T have been chosen according to Table I.

The ideal value (4.8) for the SNR neglects several degradation factors, that are actually present in real experiments, including:

1. The direction of the source may be unfavorable.

2. The frequency interval (f_b, f_e) swept by the signal is finite because the record has a finite length and the instrument has its own cutoffs.

3. The noise spectrum is generally red, which damages the SNR in the critical low frequency band.

Only experiments can provide a safe estimate of the noise structure, especially when aiming at high sensitivities or wide frequency windows. Past Doppler data can be approximated with a simple analytical expression made up with power law contributions:

$$S_n(f) = S_0 \sum_{j=1}^3 \left(\frac{f}{f_j} \right)^{\alpha_j}, \tag{4.12}$$

17

where

$$S_0 = S_n(1/T) = \sigma_y^2(T)T \tag{4.13}$$

sets the spectral level; the frequencies f_j and the exponents α_j, fulfilling

$$\sum_{j=1}^{3} (T\,f_j)^{-\alpha_j} = 1\,, \tag{4.14}$$

characterize the different contributions to the noise. We can define the transition frequencies f_{12} and f_{23} as the intercept between two power approximations; for example, the transition frequency f_{12} between region 1 and 2 (characterized by the index α_1 and α_2, respectively) is given by

$$\left(\frac{f_{12}}{f_1}\right)^{\alpha_1} = \left(\frac{f_{12}}{f_2}\right)^{\alpha_2}\,. \tag{4.15}$$

In general, high frequencies (say, above $\simeq 0.2 - 1$ Hz) are dominated by thermal noise, with the index $\alpha_3 = 2$; in the case of ULYSSES, this spectral region is also perturbed by the spacecraft rotational dynamics, so that the data have been actually low-pass filtered to 5×10^{-2} Hz $= f_{23}$ (for ULYSSES we can therefore assume $\alpha_3 \gg 1$ and we have formally achieved that by setting $\alpha_3 = 10$). The frequency window between f_{12} and f_{23} can be characterized by a power law with index $\alpha_2 \approx -0.5$, due to propagation noise [14,15]. The analysis of past experiments has been mostly confined to this band, in particular to frequencies larger than $\approx 1/T = f_{12}$; in the case of ULYSSES, the procedure for the generation of residuals essentially cuts off all frequencies below $\simeq 10^{-4}$ Hz; we have formally achieved this by adopting $\alpha_1 = -10$ (see Table II).

As we have already anticipated in the Introduction (and we shall show more in detail in the next Sections), one of the main conclusions of this paper is that low frequencies (i.e. $\lesssim 1/T$) are crucial to achieve large SNR and to widen the range of accessible masses. The noise spectrum for $fT \lesssim 1$ is to a large extent unknown, as systematic effects, mostly related to the orbit determination process and the tropospheric correction, are likely to come into play. For the goal of assessing the expected SNR for CASSINI we take the view that these systematic effects do not exceed the propagation noise above 10^{-4} Hz and keep $\alpha_2 = -0.5$. The level S_0 is given by the main specification for the Allan deviation, i.e., $\sigma_y = 3 \times 10^{-15}$ at 10^4 sec, corresponding to $S_n(10^{-4}\text{Hz}) = 9 \times 10^{-26}$ sec; we also limit our band to a minimum frequency of 10^{-6} Hz. For the interval up to $f_{12} = 10^{-4}$ Hz the only experimental evidences come from ULYSSES data, which showed an approximate behavior as f^{-2} and, accordingly, we chose $\alpha_1 = -2$; this value, however, is conservative, as in the processing of ULYSSES data no particular attention was taken at the reduction of the noise below 10^{-4} Hz. The effect of possible different values of α_1 will be explored in Sec. IV A. Thermal noise, with $\alpha_3 = 2$, can be expected to set in at about 0.1 Hz; however, the limited sampling time will prevent to go much beyond. In Fig. 5 we show the noise spectral density of CASSINI and ULYSSES, computed using Eqs. (4.12) and (4.13) with the parameters given in Table II.

Keeping S_0 and the frequencies f_j (j=1,2,3) fixed, we now write the SNR in the form

$$\rho^2 = K \frac{\mathcal{M}^{5/3} T^{4/3}}{S_0 D^2} \Upsilon(\xi_b, \xi_e, \theta; \alpha_j).\tag{4.16}$$

The *sensitivity function*

$$\Upsilon(\xi_b, \xi_e, \theta; \alpha_j) \equiv K^{-1} \left\{ \int_{\xi_b}^{\xi_e} \xi^{-7/3} \left[\sum_j \left(\frac{\xi}{\xi_j} \right)^{\alpha_j} \right]^{-1} |\tilde{r}_\theta(\xi)|^2 \, d\xi \right\}\tag{4.17}$$

measures the change of SNR with respect to the "ideal" case, Eq. (4.8), and fulfils

$$\Upsilon(0, \infty, \pi/2; 0) = 1\,.\tag{4.18}$$

Generally this function is less than unity and gives a degradation; we must however point out that the value $\pi/2$ for the angle θ is not always (i.e. for any arbitrary choice of α_j) the best; furthermore, we have defined the "white noise" considering the level of the real noise at $f = 1/T$, so that $S_n(f)$ may actually be smaller than the white noise for $f > 1/T$. Notice also that when $\alpha_1 \geq -2/3$ the SNR spectral density is not integrable and the total SNR is dominated by the low frequency end f_b.

The crucial physical parameter of a binary is its chirp mass $\mathcal{M}$, which characterizes the rate of change of the gravitational wave frequency and sets the relationship (except for class IV)

$$\begin{aligned}
\mathcal{M} &= \frac{5^{3/5}}{(8\pi)^{8/5}} T_1^{-3/5} f_b^{-8/5} \left[1 - \left(\frac{f_b}{f_e} \right)^{8/3} \right]^{3/5} \\
&= \mathcal{M}_c \left[1 - \left(\frac{f_b}{f_e} \right)^{8/3} \right]^{3/5} \qquad \text{(class I - III)}\,.
\end{aligned}\tag{4.19}$$

We see that, given f_b and T_1, there is a critical value of the chirp mass

$$\begin{aligned}
\mathcal{M}_c &= \frac{5^{3/5}}{(8\pi)^{8/5}} T_1^{-3/5} f_b^{-8/5} \\
&\simeq 9.2 \times 10^5 \left(\frac{f_b}{10^{-4}\,\text{Hz}} \right)^{-8/5} \left(\frac{T_1}{40\,\text{days}} \right)^{-3/5} M_\odot\,.
\end{aligned}\tag{4.20}$$

above which no measurement is possible, in class I-to-III. At this critical value, when $f_b \ll f_{\text{isco}}$, T_1 basically coincides with the time to coalescence τ_c.

When $\mathcal{M} \ll \mathcal{M}_c$, the signal is intrinsically narrow-band, and so are the measurements; the fractional bandwidth

$$\Delta = \frac{f_e - f_b}{f_b}\tag{4.21}$$

is small and given by

$$\Delta = \frac{3}{8} \left(\frac{\mathcal{M}}{\mathcal{M}_c} \right)^{5/3} = \frac{3}{8} \frac{T_1}{\tau_c}\,.\tag{4.22}$$

19

This case, in which there is little power and information, is less interesting.

When the data set includes the merger (class IV), instead of Eq. (4.19) we have

$$\mathcal{M} = \mathcal{M}_c \left[\frac{T_1}{\tau_c} \left(1 - \left(\frac{f_b}{f_{\text{isco}}} \right)^{8/3} \right) \right]^{3/5} \qquad (\text{class IV}).\qquad (4.23)$$

The coefficient within square brackets can be greater than unity, so that the inequality $\mathcal{M} < \mathcal{M}_c$ does not apply.

Since, with decreasing frequency, the spectral density of the SNR decreases or has a weaker growth below $1/T$, it is very convenient to have $T f_b < 1$. When $\xi_e = f_e T \ll 1$ the response $i\pi\xi \sin^2\theta$, Eq. (3.6), weakens the signal. When $\xi_e > 1$ the response introduces strong modulations that depend on θ and we have full sensitivity. This is the interesting region and will be explored in Sec. IV A using the dynamical behavior of the source.

Before discussing in detail the behavior of the SNR in observations of in-spiral signals as function of the relevant parameters, it is instructive to compare the sensitivity of Doppler experiments to the radiation emitted during the in-spiral and merger phase. If ρ_{insp} and ρ_{merg} correspond to the optimal SNR achievable by observations of the same source in the two regimes, from Eq. (4.5) we can write:

$$\frac{\rho_{\text{insp}}}{\rho_{\text{merg}}} = \left[\frac{\int_{f_{\text{B}}}^{f_{\text{isco}}} \frac{|\tilde{r}_\theta(f)|^2}{f^2 S_n(f)} \frac{dE_{\text{insp}}(f)}{df} df}{\int_{f_{\text{isco}}}^{f_{\text{qnm}}} \frac{|\tilde{r}_\theta(f)|^2}{f^2 S_n(f)} \frac{dE_{\text{merg}}(f)}{df} df} \right]^{1/2}.\qquad (4.24)$$

We stress that in the previous relationship we have assumed optimal filtering not only for the in-spiral but also for the merger signal; if for the former the assumption is realistic, cfr. [107], for the latter it is indeed very optimistic. Notice also that ρ_{insp} is the largest SNR obtainable for a chirp, as we integrate over the widest frequency band (f_B, f_{isco}) for a data set of length T_1 (cfr. Sec. IV A), and we have averaged the three-pulse response function over the angle θ, cfr. Eq (3.12). For a given source, if $(\rho_{\text{insp}}/\rho_{\text{merg}}) > 1$ (< 1) it is therefore 'more convenient' to search for it by means of observations of the in-spiral (merger) signal.

Inserting Eqs. (2.36) and (2.37) into Eq. (4.24), the ratio of SNR's becomes

$$\frac{\rho_{\text{insp}}}{\rho_{\text{merg}}} \simeq 1.1 \, J \left(\frac{\epsilon_{\text{merg}}}{0.1} \right)^{-1/2} \left(\frac{T}{10^4 \, \text{sec}} \right)^{1/6} \left(\frac{M}{2 \times 10^7 \, M_\odot} \right)^{1/3} \left(\frac{\mu}{5 \times 10^6 \, M_\odot} \right)^{-1/2}, \qquad (4.25)$$

where

$$J \equiv \left[\frac{\int_{(T f_{\text{B}})}^{(T f_{\text{isco}})} \frac{|\tilde{r}_\theta(\xi)|^2}{\xi^{7/3} S_n(\xi)} d\xi}{\int_{(T f_{\text{isco}})}^{(T f_{\text{qnm}})} \frac{|\tilde{r}_\theta(\xi)|^2}{\xi^2 S_n(\xi)} d\xi} \right]^{1/2} \qquad (4.26)$$

measures the relative overlap of the in-spiral and merger signals with respect to the instrument response. In Fig. 6 we show $(\rho_{\text{insp}}/\rho_{\text{merg}})$ and J as a function of the chirp mass for two different mass ratios, 1 and 0.01, for a nominal CASSINI experiment of 40 days with $S_n(f)$ given by Eqs. (4.12 – 4.14). The value of the chirp mass $\mathcal{M} \sim 10^7 \, M_\odot$ (for a low

20

frequency cut-off of 10^{-6} Hz) sets the transition between the systems that are more convenient to be searched during the in-spiral phase and those during the merger phase: for $\mathcal{M} > 10^7\,M_\odot$, ρ_{merg} rapidly exceeds ρ_{insp} by a factor ~ 10 or more. Assuming a low frequency cut-off around 10^{-4} Hz, as done in past experiments, the transition occurs at a lower value of $\mathcal{M} \simeq 5 \times 10^6\,M_\odot$ and the drops of $(\rho_{\mathrm{insp}}/\rho_{\mathrm{merg}})$ is much steeper. As a consequence, for $\mathcal{M} \lesssim 10^7\,M_\odot$ the neglect of the merger signal in searching templates is not serious; for $\mathcal{M} \gtrsim 10^7\,M_\odot$ coherent search techniques that include merger waveforms would rapidly increase the instrument range of sight, by more than one order of magnitude. However, at present, the radiation produced during the final burst does not seem to be the most promising signal to be searched for in Doppler experiments, as astrophysical considerations suggest that its amplitude is not large enough to dominate the noise and matched filtering techniques would fail to enhance the SNR due to the poor prior knowledge of the waveform. Only coincidence experiments can offer a chance of carrying out such searches; this work is currently in progress – under the assumption of very simple shapes of the waves – for the analysis of data recorded in coincidence during the tracking of ULYSSES, MARS-OBSERVER and GALILEO [16].

A. Sensitivity function

In this Section we discuss the dependence of the sensitivity function $\Upsilon(\xi_b, \xi_e, \theta; \alpha_j)$ on the main parameters that characterize the in-spiral signal and the instrument, in particular the conditions under which Υ attains a value close to the ideal one or, equivalently, the possible causes of degradation.

To illustrate the first reason of degradation – the unfavorable angle θ – as well as the behavior of Υ depending on the frequency range swept by the signal during the observation time, we show in Fig. 7 the sensitivity function per unit frequency $\tilde{\Upsilon}(f)$ for CASSINI's nominal noise (see Fig. 5 and Table II). The sensitivity peak lies in the interval $0.1 \lesssim \xi \lesssim 1$, and broadens and diminishes as $\cos\theta$ increases. For $\xi \ll 1$, $\tilde{\Upsilon}(f)$ is a monotonic, decreasing function of $\cos\theta$, while as ξ exceeds unity, oscillations of increasing frequency occur. The overall effect of the angle θ on Υ is given by the function $\Upsilon(\xi_e = 0, \xi_b = \infty, \theta; \alpha_1)$, plotted in Fig. 8, where we also keep α_1 as free parameter in order to show the effect of the redness of the noise spectral density at low frequencies (that is $f \lesssim 1/T$); for $\alpha_1 \gtrsim -0.9$, $\Upsilon(\xi_e = 0, \xi_b = \infty, \theta; \alpha_1)$ has a maximum at the expected value $\theta = \pi/2$. This is not true anymore for redder spectra, and the value of θ at which Υ reaches the maximum depends on α_1; for $\alpha_1 = -2$ it corresponds to $\cos\theta \simeq 0.68$.

Concerning the second reason of degradation of Υ – the limited bandwidth of the signal – we show first (Fig. 9) the effect of f_b and f_e. The deterioration can be strong: Υ can significantly deviate (by one order of magnitude or more) from the ideal value. When both ξ_b and ξ_e are $\lesssim 1$, Υ is a smooth function of f_b and f_e, but as soon as they enter the region $f \gtrsim 1/T$, there are oscillations. We have used the 'nominal' CASSINI form of the noise spectrum (Fig. 5) and we keep it fix from now on.

It is interesting to investigate Υ in relation to relevant astrophysical parameters. We concentrate on four fiducial "best" sources defined by choosing the initial frequency f_b and assuming that the coalescence occurs at the end of the record, so that $f_b = f_B$ and $f_e = f_{\mathrm{isco}}$.

Each of them is a binary with equal masses ($\eta = 1/4$), which determines the chirp mass

$$\mathcal{M} = \mathcal{M}_c \left[1 - \left(\frac{f_b}{f_{\text{isco}}} \right)^{8/3} \right]^{3/5} , \qquad (4.27)$$

in terms of the critical mass for a nominal run of 40 days, see Eq. (4.20). This sets also the final frequency $f_e = f_{\text{isco}}$ and the number of wave cycles recorded at the detector. Table III summaries the main properties of the fiducial sources. In all four cases $f_e \gg f_b$, so that we have a wide band search and the source's chirp mass is only slightly smaller than the critical value.

Keeping f_b and $\mathcal{M}$ fixed, we first study the effect of T_1 on Υ. As T_1 decreases, the signal becomes of class III and we loose a progressively greater part of its end. Insisting that the chirp mass remains the same, the final frequency f_e decreases according to Eq. (2.15). This progressive restriction of the search bandwidth is responsible for the great deterioration in Υ, and therefore in SNR, shown in Fig. 10. Since we have assumed that there is no signal beyond the coalescence frequency f_{isco}, the sensitivity function remains constant for $T_1 > 40$ days.

In Fig. 11 we show how the sensitivity function is affected by the round-trip light-time T, for the same fiducial sources (and with a run of 40 days) . The variation of T deplaces the three-pulse response function – Eq. (3.9) and Fig. 7 – in relation to the search band (f_b, f_e). The deterioration with increasing T is due to the fact ξ_e becomes smaller than unity and one looses signal from the high frequency side.

Finally, in Fig. 12 we investigate the effect of f_b (that is the epoch of the binary life at which the instrument is "turned on") on Υ; for each value of f_b, we have in fact computed the corresponding critical chirp mass (4.20) for a 40-day experiment and then evaluated the sensitivity function for three different source's orientation in the sky; essentially, for each f_b we tune the observation on the mass that produces the highest SNR. The largest values of Υ are achieved for $10^{-5} \, \text{Hz} \lesssim f_b \lesssim 10^{-3} \, \text{Hz}$, corresponding to $10^4 \, M_\odot \lesssim \mathcal{M}_c \lesssim 10^8 \, M_\odot$.

B. Sensitivity of past and future Doppler experiment

In this Section we analyze the sensitivity of Doppler experiments – in particular CASSINI – to search for in-spiral signals; we estimate the range of sensitivity and the achievable signal-to-noise ratio as function of the chirp mass $\mathcal{M}$ and the initial frequency f_b (as well as η). We consider in detail two targets, the Virgo Cluster ($D \simeq 17 \, \text{Mpc}$) and the Galactic Centre ($D \simeq 8 \, \text{kpc}$); the results are presented so that they can be scaled to an arbitrary distance and location in the sky.

CASSINI will perform three experiments, each lasting 40 days at the epoch of three solar oppositions, i.e. when the Sun, the Earth and the probe are approximately aligned, in this order, so as to minimize the noise due to interplanetary plasma (see Table I and Fig. 13) [18]. The main tracking will be done in X band from the operational antennas of NASA's Deep Space Network (DSN), and in K_a band from the new experimental DSN station DSS25 at Goldstone (California). Another advanced station to be build in Sardinia (the Sardinia Radio Telescope) has been recently funded and it is hoped that it will track

CASSINI in K_a-band (up and down) and X-band (down). The radio system of CASSINI's mission has a specification for the overall Allan deviation in K_a band of 3×10^{-15}, for integration times between 1000 and 10,000 sec, one-to-two orders of magnitude better than previous experiments. In addition, the sensitivity will be improved, with respect to past missions, by the longer time of observation and, possibly, by the combination of the three records. Fig. 13 shows the round-trip light-time and the value of $\cos \theta$ for the Virgo Cluster and the Galactic Centre during the cruise of the space-probe to Saturn.

We begin by investigating the expected SNR produced by in-spiraling signals of possible sources located in the Virgo Cluster in the plane $(\mathcal{M}, f_b)$. Since it turns out that the three planned experiments have comparable sensitivities, we give explicit results only for the last one, in 2004. Fig. 14 shows for the Virgo Cluster three different levels of SNR: $\rho = 1, 5$ and 10. It confirms the theoretical suggestion that the detectable events of class III lie in a narrow strip below the critical value of the chirp mass. All events above it are of class IV and include the merger. This plot shows how the SNR changes as function of both $\mathcal{M}$ and f_b: at $\rho = 1$ and for black holes of comparable masses, the smallest detectable chirp mass is $\simeq 5 \times 10^5 \, M_\odot$. Lower masses are excluded because the systems are too far from coalescence and masses larger than $\sim 10^9 \, M_\odot$ are not accessible because their emission frequencies are too low. Note the drastic curtailment if a low frequency cut off at $1/T \sim 10^{-4}$ Hz is assumed, as it was done in the past with ULYSSES; the strongest signals fall below $f_b T = 1$. The SNR is very much reduced when a small mass ratio is assumed (lower panel); an important and unknown factor in assessing the detectability of gravitational radiation from MBHB's is the statistics of this ratio.

One wonders if a source in the Virgo cluster detected in the last opposition is traceable also in the second or the first (albeit at a smaller SNR), thus adding important phase information. We checked that for $T_1 = 40$ days this is not the case: detectable sources are too near coalescence, in relation to the (roughly) one year separation between different runs. We have then tried doubling the observation time to $T_1 = 80$ days ('extended' experiments) and interestingly found that for some sources the three extended data sets can be combined: the strongest sources detectable in one opposition are also visible in the previous one. A single, extended experiment does not show drastic improvements over the nominal record; however, the accessible portion of the plane $(\mathcal{M}, f_b)$ becomes slightly wider. Of course, a drastic improvement in sensitivity and detection probability would be expected for a continuous run of a few years.

How far is the farthest detectable system? From Fig. 15 we see that the highest SNR, about 28, produced by a source in the Virgo cluster is attained for a system of comparable masses $\simeq 5 \times 10^7 \, M_\odot$; at $\rho = 1$ this corresponds to a distance ≈ 600 Mpc; if $M_2/M_1 = 10^{-2}$, the ken is reduced by a factor $\simeq 5$.

In order to have an idea of the change in SNR due to different angles θ, in Fig. 16 we have studied this dependence for the third experiment in three different cases: $\mathcal{M} = 10^6, 10^7$ and $10^8 \, M_\odot$ ($f_b = f_B$, $f_e = f_{\text{isco}}$ and $\eta = 1/4$). Note that, for $\mathcal{M} = 10^6 \, M_\odot$, $\cos \theta = 0$ is a local minimum, rather than the expected maximum: this is due to the fact that signals fall in one of the high frequency minima of the three-pulse response, see Figs. 4 and 7. Figs. 14, 15 and 16 therefore allow to have an overall picture of the all-sky sensitivity of CASSINI, see Eqs. (4.16) and (4.17).

We turn now to galactic observations and consider a binary system in the centre of Our

Galaxy composed of a primary black hole of mass $M_1 = 2 \times 10^6 \, M_\odot$, whose existence is strongly inferred from observations carried out over the past 25 years [55], and a secondary, smaller object of mass M_2. In Fig. 17 we show for the third CASSINI opposition the SNR contour levels $\rho = 1, 5, 100$ in the plane (M_2, f_b). Of course, there is no signal above $f_{\text{isco}} \simeq 2 \times 10^{-3} \, (M_1/2 \times 10^6 \, M_\odot)^{-1} \, \text{Hz}$, cfr. Eq. (2.13), essentially independent of M_2. CASSINI proofs to be a fairly sensitive instruments for such signals; in fact, each of the three experiments is sensitive to secondary objects of mass down to $\sim 10 - 50 \, M_\odot$ and for $M_2 \gtrsim 100 \, M_\odot$ the expected SNR can be $\gg 10$, see Fig. 18. Remarkably, most of the sources visible during one experiment are detectable also in the others; in fact the time to coalescence is $\simeq 2995 \, (f_b/5 \times 10^{-4} \, \text{Hz})^{-8/3} \, (100 \, M_\odot/\mu) \, (2 \times 10^6 \, M_\odot/M)^{2/3}$ days (cfr. also Fig. 19). If a candidate signal in spotted in one of the data sets, it is therefore possible to chase it also in the other oppositions, which provides a robust method of accepting or discarding candidate events by coherently tracking the gravitational phase over a period of some years. This is a direct consequence of the fact that many signals would be recorded as class II and III (therefore far from the final coalescence) as is shown in Fig. 17 by the dotted and dashed line in the plane (M_2, f_b); this is in contrast with what appends for observations in the Virgo cluster, where most of the signals show up as class IV. The good sensitivity for nearby sources allows also to search for possible binary systems in other galaxies of the Local Group.

It is interesting to compare CASSINI's sensitivity with past Doppler experiments (Table I). The best Doppler data available today come from observations carried out in 1991, 1992 and 1993 with the probes ULYSSES, GALILEO and MARS-OBSERVER. In 1993 all three spacecraft have been simultaneously tracked for about two weeks, with a triple coincidence experiment whose data are being analyzed; this experiment will be useful to search for signals coming from the merger phase [16].

We concentrate on ULYSSES' 1992 experiment [14,15]. After pre-processing, only 14 days of data have been retained, centered around the sun opposition. Their Allan deviation (at 1000 sec) is variable, with only its best value near the specification, 3×10^{-14}. Data outside the bandwidth $\simeq 2.3 \times 10^{-4} - 5 \times 10^{-2} \, \text{Hz}$ have been discarded, see Fig. 5: at high frequency they are corrupted by the anomalous rotation of the spacecraft; at low frequency, the subtraction of orbital and media contributions was carried out with a fit, which made the data unreliable below $f \simeq 1/T$. In the intermediate band the noise spectrum is well approximated by a power-low $\propto f^{-0.5}$ (see Table II). The low frequency cut off limits the largest observable mass to

$$\mathcal{M} \lesssim 9 \times 10^6 \, (4 \, \eta)^{3/5} \, M_\odot \,, \tag{4.28}$$

and the value of the critical chirp mass (4.20) for the 14-days ULYSSES second opposition experiment is

$$\mathcal{M} \simeq 1.3 \times 10^5 \left(\frac{f_b}{5 \times 10^{-4} \, \text{Hz}} \right)^{-8/5} \left(\frac{T_1}{14 \, \text{days}} \right)^{-3/5} M_\odot \,; \tag{4.29}$$

Eqs. (4.28) and (4.29) clearly indicate that the most interesting region in the $(\mathcal{M}, f_b)$ plane is not accessible (cfr. Fig. 14) and therefore the largest attainable distance is strongly reduced. Moreover, the noise spectral density, as defined by Eqs. (4.12)–(4.15) with the

parameters reported in Table II (see Fig. 5), is about two orders of magnitude larger than for CASSINI. According to Eq. (4.10), the ideal *ken* (we recall that it is defined for $\rho_{id} = 1$) holds

$$D_{id} \simeq 1 \left(\frac{\mathcal{M}}{1.3 \times 10^5 M_\odot} \right)^{5/6} \left(\frac{S_0}{2.5 \times 10^{-24}\,\mathrm{Hz}^{-1}} \right)^{-1/2} \left(\frac{T}{4430\,\mathrm{sec}} \right)^{2/3} \mathrm{Mpc}\,. \qquad (4.30)$$

Therefore, in conventional astrophysical scenarios, ULYSSES' experiments are relevant only for the Galactic Centre, whose angular position with respect to the spacecraft was $\theta \approx 109^o$. It is straightforward to check that at $\rho = 5$ secondary black holes with $M_2 \gtrsim 10^3\,M_\odot$ would be detectable.

V. CONCLUSIONS

We have analyzed the sensitivity of Doppler detectors to gravitational waves emitted by coalescing binaries in their in-spiral phase. For CASSINI's experiments sources in the Virgo Cluster would be observable at a signal-to-noise ratio up to $\simeq 30$. Furthermore, binary systems with $M_1 \sim M_2 \sim 5 \times 10^7\,M_\odot$ at distance $\sim 600\,\mathrm{Mpc}$ are within the range of the instrument. If in the centre of Our Galaxy there is a massive black hole of $2 \times 10^6\,M_\odot$, orbiting black holes with mass $\gtrsim 50\,M_\odot$ would be easily detectable; for larger masses the signal-to-noise ratio can be considerably higher and therefore one can reach other galaxies within the Local Group. These are considerable improvements in sensitivity and range of accessible masses with respect to past Doppler experiments.

This analysis has been made in relation to astrophysically reasonable sources, but without any concern for the probability of such events and their detection. Considering our ignorance about sources of gravitational waves, in particular for events in galactic nuclei, this point of view appears reasonable, especially for non dedicated experiments like CASSINI's; however, it is healthy and sobering to assess what one can predict on the basis of *very simple and conventional astrophysical models*. The estimation of the event rate is a much debated problem in low frequency gravitational wave experiments (see [19,32,35,36,39] and reference therein), with sensitivity not good enough to detect signals from known stellar mass galactic binaries. We briefly consider here two models: (a) accretion of small black holes onto a massive one in a galactic core and (b) coalescence of two MBHB's of comparable mass, possibly resulting from the mergers of two galaxies. In the context of Doppler experiments, they are appropriate to small and large distances, respectively.

Let consider now case (a). Suppose that a central black hole M in a typical galaxy (i.e., in Our Galactic Centre) has captured $N = M/M_2$ masses M_2 at the uniform rate $R = H_0 M/M_2$ during the whole life of the Universe $H_0^{-1} \simeq 10^{10}\,h_{100}\,\mathrm{yr}$, where h_{100} is the Hubble constant normalized to $100\,\mathrm{km\,sec}^{-1}\,\mathrm{Mpc}^{-1}$; each of these captures gives rise to a chirp. In this ideal case, in which the spread in mass is neglected, one could consider the search as follows. For a given M_2 (and fixed M_1, which determine uniquely the chirp mass) there is a characteristic initial frequency f_B, given by Eq. (2.18), for which we have a wide band detection and coalescence at the end of the record; this corresponds to the situation in which the SNR is maximum. As f_b diminishes, the fractional bandwidth Δ – see Eq. (4.21) – decreases according to

$$f_b \simeq f_B[1 - (1 - \Delta)^{-8/3}]^{3/8} \,, \tag{5.1}$$

and so does the SNR, proportionally to Δ:

$$\rho^2 \simeq \rho_{\rm id}^2 \, K^{-1} \, \tilde{\Upsilon}(f) \, f \, \Delta \,, \tag{5.2}$$

where $f \sim f_b \sim f_e$. Since a small value of Δ increases the useful time for detection $T_{\rm D}$ – that is the total time for which the source is "visible" above the detection threshold $\rho_{\rm D}$ – detection will generally occur at a SNR less than the maximum (attained for $f_b = f_B$ and $f_e = f_{\rm isco}$) and with a start frequency $f_b < f_B$. $\rho_{\rm D}$ determines the threshold $\Delta_{\rm D}$ for the fractional bandwidth and $T_{\rm D}$, via Eq. (4.22). Indeed, the success probability is $P = R \, T_{\rm D}$ and we have computed it using the results reported in Fig. 17. Its behavior as a function of the mass M_2, which enters through both R and $T_{\rm D}$, is given in Fig. 19 for the thresholds $\rho_{\rm D} = 1$, 5, 10 and 15. This allows us to determine the most favorable value of M_2, about $100 \, M_\odot$, and the corresponding (optimistic!) success probability, in each experiment of $T_1 = 40$ days, is $\sim 10^{-5}$.

We turn now to case (b). To go to very large distances and to reach the largest number of sources, we must aim at large masses and use low frequencies, in the band $f \, T \lesssim 1$. In this frequency range, the noise spectral density is well described by a single power low

$$S_n(f) \simeq S_0 \left(\frac{f}{f_1}\right)^{\alpha_1} \,. \tag{5.3}$$

The SNR produced by a source that sweeps the bandwidth Δ, where $\xi_e = (1 + \Delta) \, \xi_b$, see Eq. (4.21), can be analytically computed from Eq. (4.16) assuming the simple low-frequency behavior of the Doppler response filter (3.10):

$$\rho^2 = k \, \frac{T^{4/3} \, \mathcal{M}^{5/3}}{S_0 \, D^2} \, (T \, f_1)^{\alpha_1} \, (T \, f_b)^{(2/3 - \alpha_1)} \left[(1 + \Delta)^{(2/3 - \alpha_1)} - 1\right] \,; \tag{5.4}$$

k is a numerical coefficients that depends on the angles $\iota \,, \varphi$ and θ. The largest attainable distance, in observations of a binary of mass $\mathcal{M}$ is therefore

$$D = k^{1/2} \, \frac{T \, \mathcal{M}^{5/6}}{S_0^{1/2} \, \rho} \, f_1^{\alpha_1/2} \, f_b^{(1/3 - \alpha_1/2)} \left[(1 + \Delta)^{(2/3 - \alpha_1)} - 1\right]^{1/2} \tag{5.5}$$

and the corresponding number of detectable events

$$\begin{aligned} N &\sim R \, T_1 \, (D \, H_0)^3 \\ &= R \, T_1 \, H_0^3 \, k^{3/2} \, \frac{T^3 \, \mathcal{M}^{5/2}}{S_0^{3/2} \, \rho^3} \, f_1^{3 \, \alpha_1/2} \, f_b^{1 - 3 \, \alpha_1/2} \left[(1 + \Delta)^{2/3 - \alpha_1} - 1\right]^{3/2} \,. \end{aligned} \tag{5.6}$$

Of course, the range of the instrument depends also on the mass of the source and one can express $\mathcal{M}$ as a function of f_b, T_1 and Δ, using Eq. (4.19); Eq. (5.6) therefore becomes:

$$\begin{aligned} N &= R \, H_0^3 \, k' \, \frac{T^3 \, \mathcal{M}^{5/2}}{S_0^{3/2} \, T_1^{1/2} \, \rho^3} \, f_1^{(3 \, \alpha_1/2)} \, f_b^{-3 \, (1 + \alpha_1/2)} \\ &\quad \times \left\{\left[(1 + \Delta)^{(2/3 - \alpha_1)} - 1\right] \left[1 - (1 + \Delta)^{-8/3}\right]\right\}^{3/2} \,, \end{aligned} \tag{5.7}$$

where k' is a numerical constant depending on k. We see that N is proportional to $f_b^{-3(1+\alpha_1/2)}$ and increases with decreasing frequencies if $\alpha_1 < -2$. The nominal case $\alpha_1 = -2$ (Table II) marks the transition between the two alternatives, whether it is useful or not to go to lower frequencies. If we assume (naively and optimistically) that each galaxy in the Universe contains a massive black hole and has undergone N_m merging events leading to the formation of a binary with time to coalescence shorter than the Hubble time, we can estimate the event rate as $R = N_m N_g / H_0$, where N_g is the total number of galaxies. As we have seen in the previous section, the *ken* of CASSINI is $D \sim 600\,\mathrm{Mpc}$ and therefore the probability of detection is

$$P \sim 10^{-1}\, N_m \left(\frac{3\,T_1}{120\,\mathrm{days}} \right) \left(\frac{D}{600\,\mathrm{Mpc}} \right)^3 \left(\frac{H_0^{-1}}{3\,\mathrm{Gpc}} \right)^{-3}. \tag{5.8}$$

Of course, larger distances could be attained if we knew the waveform produced during the final collapse and the merger could be included in the search. In the present situation of ignorance, however, a good level of confidence in the detection of merger signals requires coincidence experiments.

We conclude that, in conventional astrophysical scenarios, the events we are looking for do not have a large probability to be detected, the extragalactic case (b) being more favorable. Note, however, that for low chirp mass sources $\mathcal{M} \sim 100\,M_\odot$, the total SNR could be increased by combining two or three records.

Present Doppler experiments are relatively cheap, but use non dedicated spacecraft and are limited in instrumentation, orbits, observation time and by several other constraints. However, despite their low sensitivity, they are the only one that at present can access the coalescence of binaries involving massive objects, and therefore quite valuable. They might discover gravitational waves; if they do not, they will provide interesting astrophysical limits on massive sources, in particular in Our Galactic Centre, the Local Group and the Virgo Cluster. Since real data are already available in large amounts and the search techniques are very similar to those implemented for Earth-based (and, in future, space-borne) laser interferometers, Doppler experiments can also be used to test filtering and processing techniques.

REFERENCES

[1] A. Abramovici et al., Science **256**, 325 (1992).

[2] C. Bradaschia et al., Nucl. Instrum. Methods Phys. Res. A **289**, 518, (1990).

[3] K. Danzmann, in *Gravitational Wave Experiments*, edited by E. Coccia, G. Pizzella and F. Ronga (World Scientific, Singapore, 1995), pp. 100–111.

[4] K. Tsubono, in *Gravitational Wave Experiments*, edited by E. Coccia, G. Pizzella and F. Ronga (World Scientific, Singapore, 1995), pp. 112–114.

[5] P. Astone et al., Phys. Lett. B **385**, 421 (1996).

[6] P. Astone et al., Astropart. Phys. **7**, 231 (1997).

[7] M. Cerdonio et al., in *Gravitational Wave Experiments*, edited by E. Coccia, G. Pizzella and F. Ronga (World Scientific, Singapore, 1995), pp. 176–194.

[8] E. Mauceli, Z.K. Geng, W, O. Hamilton, W. W. Jhonson, S. Merkowitz, A. Morse, B. Price and N. Solomonson Phys. Rev. D **54**, 1264 (1996).

[9] Blair et al. in *Gravitational Wave Experiments*, edited by E. Coccia, G. Pizzella and F. Ronga (World Scientific, Singapore, 1995), pp. 144–160.

[10] F. B. Estabrook and H. R. Wahlquist, Gen. Rel. Grav. **6**, 439 (1975)

[11] R.W. Hellings, P.S. Callahan and J.D. Anderson Phys. Rev. D **23**, 844 (1991).

[12] J.D. Anderson, J.W. Armstrong and F.B. Estabrook et al., Nature **308**, 158 (1984).

[13] J.W. Armstrong, F.B. Estabrook and H.D. Wahlquist, Astrophys. J. **318**, 536 (1987).

[14] B. Bertotti et al., Astron. and Astroph. Suppl. Series **92**, 431 (1992).

[15] B. Bertotti, R. Ambrosini, J. Armstrong, S.W. Asmar, G. Comoretto, G. Giampieri, Y. Koyama, L. Iess, A. Messeri, A. Vecchio and H.D. Whalquist, Astron. and Astrophys. **296**, 13, (1995).

[16] J. W. Armstrong, *The GALILEO/MARS OBSERVER/ULYSSES coincidence experiment*, to be published in *Second Amaldi Conference on Gravitational Waves*, ed. E. Coccia et al. (World Scientific, Singapore); L. Iess, J.W. Armstrong, B. Bertotti, H.D. Wahlquist and F.B. Estabrook *Search for gravitational wave bursts by simultaneous Doppler tracking of three interplanetary spacecraft*, talk presented at the *15th International Conference of General Relativity and Gravitation*, Pune 16-21 Dec. 1997.

[17] CASSINI mission: References and Information on WWW at http://www.jpl.nasa.gov/cassini.

[18] G. Comoretto, B. Bertotti, L. Iess and R. Ambrosini, Nuovo Cim. **15C**, 1193 (1992).

[19] P. Bender et al., *LISA Pre-Phase A Report*, MPQ 208 (1995).

[20] R. W. Hellings, Ω *Orbiting Medium Explorer for Gravitational Astrophysics*, Mixed Proposal (1995).

[21] B. Bertotti, *Gravitational wave detection from Space*, to be published in the *Proceedings of the 14th International Conference on General Relativity and Gravitation*.

[22] K.S. Thorne, in *Proceedings of the Snowmass 95 Summer Study on Particle and Nuclear Astrophysics and Cosmology*, edited by E.W. Kolb and R. Peccei (World Scientific, Singapore, 1995).

[23] K.S. Thorne, in *Black holes and relativity*, edited by R. Wald (University of Chicago Press, Chicago), in press; preprint gr-qc/9706079.

[24] K.S. Thorne and V.B. Braginsky, Astrophys. J. **204**, L1 (1976).

[25] V. M. Lipunov, K. A. Postnov, Soviet Astr. **31**, 228 (1987).

[26] V. M. Lipunov, K. A. Postnov, and M. E. Prokhorov Soviet Astr. **31**, 228 (1987).

[27] D. Hils, P. L. Bender, and R.F. Webbink, Astrophys. J. **360**, 75 (1990).

[28] R. A. Hulse, Rev. Mod. Phys. **66**, 699 (1994).

[29] J. H. Taylor, Rev. Mod. Phys. **66**, 711 (1994).

[30] J. H. Taylor and J. M. Weisberg, Astrophys. J. **345**, 434 (1989).

[31] D. Hils and P. L. Bender, Astrophys. J. **445**, L7 (1995).

[32] S. Sigurdsson and M. J. Rees, Mont. Not. Royal Astron. Soc. **284**, 318 (1996)

[33] M. Shibata, Phys. Rev. D **50**, 6297 (1994).

[34] M.C. Begelman, R.D. Blandford & M.J. Rees, Nature **287**, 307 (1980).

[35] M.G. Haehnelt, Mont. Not. Roy. Astron. Soc. **269**, 199 (1994).

[36] A. Vecchio, Class. and Quantum Grav. **14**, 1431 (1997).

[37] R. R. Caldwell and B. Allen Phys. Rev. D **45**, 3447 (1992).

[38] G. Giampieri & A. Vecchio, General Relat. and Gravitation, **27**, 793 (1995).

[39] P. L. Bender and D. Hils, Class. and Quantum Grav. **14**, 1439 (1997).

[40] K. A. Postnov and M. E. Prokhorov, Astrophys. J. **494**, in press (1998).

[41] D. I. Kosenko and K.A. Postnov, *On the gravitational wave noise from unresolved extragalactic binaries*, preprint astro-ph/9801032.

[42] M. J. Rees, Proc. Nat. Acad Sci. **90**, 4840 (1993).

[43] M. Haehnelt and M. J. Rees, Mont. Not. Royal Astr. Soc **263**, 168 (1993).

[44] A. Loeb and F. A. Rasio, Astrophys. J. **432**, 52 (1994).

[45] Y. B. Zel'dovich and I. D. Novikov, Sov. Phys. Dokl. **158**, 811 (1964).

[46] E. E. Salpeter, Astrophys. J. **204**, L1 (1964).

[47] R. D. Blandford, in *Active Galactic Nuclei*, edited by T. Courvoisier and M. Mayor (Springer – Verlag, Berlin, 1990).

[48] D. E. Osterbrock, Astrophys. J. **404**, 551 (1993).

[49] M. J. Rees, Science **247**, 817 (1990).

[50] J. Kormendy and D. Richstone, Ann. Rev. Astron. Astrophys. **33**, 581 (1995).

[51] S Tremaine, in *Some unsolved problems in astrophysics*, edited by J. Bahcall and J.P. Ostriker (Princeton University Press, 1996).

[52] van der Marel, in *New light on galactic evolution*, edited by R. Bander and R. Davies (Kluwer, 1996).

[53] M. J. Rees, in *Black holes and relativity*, edited by R. Wald (University of Chicago Press, Chicago), in press; preprint astro-ph/9701161.

[54] M. Miyoshi, J. Moran, J. Herrnstein, L. Greenhill, N. Nakai, P. Diamond and M. Inoue, Nature **373**, 127 (1995).

[55] A. Eckart and R. Genzel, Nature **383**, 415 (1996).

[56] E. Maoz, Astrophys. J. **447**, L91 (1996).

[57] E. Maoz, *Dynamical constraints on alternatives to massive black holes in galactic nuclei*, Astrophys. J. Lett., in press; preprint astro-ph/9710309.

[58] J. E. Barnes and L. Hernquist, Ann. Rev. Astron. Astrophys. **30**, 705 (1992).

[59] U. Fritze - von Alvensleben, in *From Stars to Galaxies*, edited by C. Leitherer, U. Fritze - von Alvensleben and J. Huchra.

[60] N. Roos, Astron. Astrophys. **104**, 218 (1981).

[61] C. M. Gaskell, in *Jets from Stars and Galaxies*, edited by W. Kundt (Springer, Berlin, 1996) pagg. 165-196.

29

[62] N. Roos, J. S. Kastra and C. A. Hummel, Astrophys. J. **409**, 130 (1993).

[63] A. Sillanpää, S. Haarala, M. J. Valtonen, B. Sundelius and G. G. Byrd, Astrophys. J. **325**, 628 (1988).

[64] L. Valtoja, M. J. Valtonen and G. G. Byrd, Astrophys. J. **343**, 47 (1989).

[65] C. M. Gaskell, Astrophys. J. **646**, L107 (1996).

[66] E. Poisson, Phys. Rev. D **54**, 5939 (1996).

[67] F. D. Ryan, Phys. Rev. D **56**, 1845 (1997).

[68] P.C. Peters, Phys. Rev.1 **136**, B1224 (1964).

[69] S. Mikkola and M. J. Valtonen, Mon. Not. R. Astron. Soc. **259**, 115 (1992).

[70] A. G. Polnarev and M. J. Rees, Astron. Astrophys. **283**, 301 (1994).

[71] A. Vecchio, M. Colpi and A. G. Polnarev, Astrophys. J. **433**, 733 (1994).

[72] H. D. Wahlquist, General Relat. Gravit. **19**, 1101 (1887).

[73] B.F. Schutz, in *The Detection of Gravitational Waves*, edited by D. Blair (Cambridge University Press, Cambridge, England, 1989), pp. 406-427.

[74] B.F. Schutz, *Introduction to the data analysis of low frequency gravitational wave data*, to be published in the *Proceedings of the 1997 Alpbach Summer School on Fundamental Physics in Space*, ed A. Wilson (ESA, 1997); preprint AEI-044.

[75] S. Smith, Phys. Rev. D, **36**, 2901 (1987).

[76] J.D. Anderson, F.B. Estabrook and H. D. Wahlquist, Astrophys. J., **318**, 536 (1987).

[77] M. Tinto & J.W. Armstrong, Astrophys. J., **372**, 545 (1991).

[78] B.F. Schutz, Nature **323**, 310 (1986).

[79] M. Tinto, Phys. Rev. D **53**, 5354 (1996).

[80] In order to extract the signal in a reliable and accurate way, the wave phase needs to be modelled including post-Newtonian correction terms [81,82]. The phase evolution is currently known, in the finite mass case, up to the post$^{2.5}$-Newtonian order [83–87]. The post^3-Newtonian terms seem also to be under control now [88,89].

[81] C. M. Will, in *Relativistic Cosmology*, edited by M. Sasaki (Universal Acad. Press, Japan, 1994), p 83.

[82] L. Blanchet, *Gravitational radiation from relativistic sources* lecture given at the *Les Huches School on Gravitational Radiation*, preprint gr-qc/9607025.

[83] L. Blanchet, T. Damour, B.R. Iyer, C.M. Will and A.G. Wiseman, Phys. Rev. Lett. **74**, 3515 (1995).

[84] L. Blanchet, T. Damour and B.R. Iyer, Phys. Rev. **D51**, 5360 (1995).

[85] C.M. Will and A.G. Wiseman, Phys. Rev. **D54**, 4813 (1996).

[86] L. Blanchet, B.R. Iyer, C.M. Will and A.G. Wiseman, Class. Quantum. Gr. **13**, 575, (1996).

[87] L. Blanchet, Phys. Rev. **D54**, 1417 (1996).

[88] L. Blanchet, *On the multiple expansion of the gravitational wave field*, preprint gr-qc/9801101.

[89] L. Blanchet, B.R. Iyer, B. Joguet, in preparation.

[90] Misner, C.W., Thorne, K. S. & Wheeler J. A. 1973. "Gravitation", W.H. Freeman and Company, New York.

[91] The angles φ and ι can be regarded as constant only in the limit of negligible spins; otherwise the coupling of the black hole spins with the binary orbital angular momentum (the so-called *spin-orbit* and *spin-spin couplings*) causes the orbital plane to

precess, which induces amplitude and phase modulations [92,93]. In the lowest-order Newtonian quadrupole approximation, that we are considering here, these effects do not appear and, accordingly, we will ignore them.

[92] T. A. Apostolatos, C. Cutler, G. S. Sussman & K. S. Thorne Phys. Rev. D **49**, 6274 (1994).

[93] L.E. Kidder, Phys. Rev. D **52**, 821 (1995).

[94] E. Seidel, *Numerical Relativity*, to be published in the *Proceedings of the 15th International Conference on General Relativity and Gravitation*.

[95] Numerical Relativity Grand Challenge Alliance, 1995. References and Information on WWW at http://jean-luc.ncsa.uiuc.edu/GC.

[96] J. Pullin, *Colliding black holes: Analytic insights*, to be published in the *Proceedings of the 15th International Conference on General Relativity and Gravitation*, preprint gr-gc/9803005.

[97] J. K. Blackburn and S. Detweiler, Phys. Rev. D **46**, 2318 (1992).

[98] L.E. Kidder, C.M. Will, and A.G. Wiseman, Phys. Rev. D **47**, 3281 (1993).

[99] L.E. Kidder, C.M. Will, and A.G. Wiseman, Class. Quant. Grav. **9**, L125 (1993).

[100] G. B. Cook, Phys. Rev. D **50**, 5025 (1994).

[101] The inequalities in Eqs. (2.19) – (2.21) are slightly pessimistic because they consider the total frequency change from the beginning frequency, while one could consider the frequency change from the middle frequency and obtain a value about two times smaller, as we have done in [15].

[102] C. Cutler and E.E. Flanagan, Phys. Rev. D **49**, 2658 (1994).

[103] E. Flanagan and S. Hughes, preprints gr-qc/9701039 and gr-qc/9710129.

[104] L. L. Smarr, in *Sources of Gravitational Radiation*, ed. by L. L. Smarr (Cambridge University Press, Cambridge, England, 1979).

[105] J. W. Armstrong, in *Gravitational Wave Data Analysis*, ed. by B. F. Schutz (Kluwer), pp. 153 (1989)

[106] J. A. Barnes et al. IEEE Trans. Instr. Meas. **IM-20**, 105 (1971).

[107] T. Damour, B. R. Iyer and B. S. Sathyaprakash, Phys. Rev. D **57**, 885 (1998).

TABLES

TABLE I. Summary of Doppler experiments to search for gravitational waves. T_1 is the effective length of data available; σ_y the average effective Allan variance of the data and T the average round-trip light-time of the radio link during the data acquisition runs. The frequency bands of the up-link (S: $2.1\,\text{GHz}$, X: $7.2\,\text{GHz}$, K_a: $34\,\text{GHz}$) and down-link (S: $2.3\,\text{GHz}$, X: $8.4\,\text{GHz}$, K_a: $32\,\text{GHz}$) carriers are shown in the two final columns. For the four short experiments carried out with PIONEER 10 and 11 and VOYAGER 1 see [21] and references therein.

Space-probe	T_1/days	σ_y	T/sec	up-link	down-link
ULYSSES 3-Dec-90/4-Jan-91	3.5	3×10^{-14}	600	S	S,X
ULYSSES 20-Feb-92/18-March-92	14	7×10^{-14}	4430	S	S,X
ULYSSES Mar-93/Apr-93	19	1.4×10^{-13}	4100	S	S,X
GALILEO Mar-93/Apr-93	19	2.3×10^{-13}	945	S	S
MARS-OBSERVER Mar-93/Apr-93	19	5×10^{-14}	1150	X	X
CASSINI 26-Nov-01/5-Jan-02	40	3×10^{-15}	5783	X, K_a	X, K_a
CASSINI 7-Dec-02/16-Jan-03	40	3×10^{-15}	7036	X, K_a	X, K_a
CASSINI 15-Dec-03/24-Jan-04	40	3×10^{-15}	7859	X, K_a	X, K_a

TABLE II. Characteristic parameters of the ULYSSES and CASSINI noise spectral density. The table shows the reference frequency $1/T$; the reference noise spectral density level $S_0 = S_n(1/T)$; the transition frequencies f_{12}, f_{23}; the exponents α_j and the frequencies f_j ($j = 1, 2, 3$) of each regime, see Eqs. (4.12) – (4.14). When, as in our case, $T f_{12} = 1$, $T f_{23} \gg 1$ and $\alpha_3 > \alpha_2$ then $T f_1 = 2^{1/\alpha_1}$, $T f_2 = 2^{1/\alpha_2}$ and $T f_3 = T f_{23} \, 2^{1/\alpha_3} \, (T f_{23})^{-\alpha_2/\alpha_3}$.

parameters	ULYSSES	CASSINI
$(1/T)/$Hz	2×10^{-4}	10^{-4}
$S_0/$Hz^{-1}	2.5×10^{-24}	9×10^{-26}
$f_{12}/$Hz	2×10^{-4}	10^{-4}
$f_{23}/$Hz	5×10^{-2}	10^{-1}
$f_1/$Hz	2×10^{-4}	7.07×10^{-5}
$f_2/$Hz	8×10^{-4}	2.5×10^{-5}
$f_3/$Hz	5×10^{-2}	7.95×10^{-1}
α_1	-10	-2
α_2	-1/2	-1/2
α_3	10	2

TABLE III. Main properties of the four fiducial sources used in the text. The assignment of the initial frequency f_b, in the case of equal masses and coalescence at the end of the record, determines the final frequency f_e (for a 40 days run), the chirp mass $\mathcal{M}$ and the number of wave cycles $\mathcal{N}$ recorded at the instrument while the signal sweeps the frequency interval (f_b, f_e).

$f_b/$Hz	$f_e/$Hz	$\mathcal{M}/M_\odot$	$\mathcal{N}$
10^{-5}	5.3×10^{-5}	3.6×10^7	52
5×10^{-5}	6.9×10^{-4}	2.9×10^6	273
10^{-4}	2.1×10^{-3}	9.2×10^5	550
5×10^{-4}	2.7×10^{-2}	7.1×10^4	2761
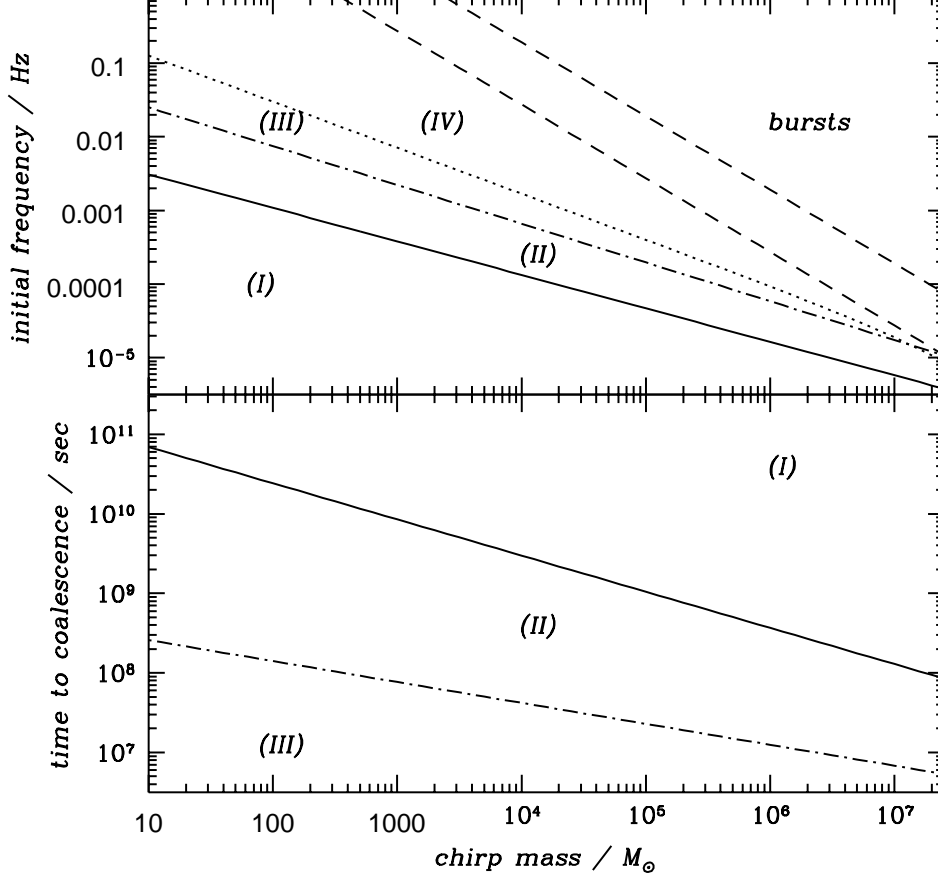
FIG. 1.   Classes of coalescing binary signals for one of the three CASSINI's experiments ($T_1 = 40\,\text{days}$). The upper panel shows the partition of the plane $(\mathcal{M}, f_b)$ in periodic (I), linear (II) and non-linear region. The dotted line divides non-linear chirps in signals of class III and IV. The dashed lines indicate the boundary between signals of class IV and bursts – i.e. f_isco as a function of $\mathcal{M}$ – for $M_2/M_1 = 0.01$ (lower line) and 1 (upper line). The lower panel shows the Newtonian times to coalescence τ_n, Eq. (2.23), computed at the transition frequency (see upper panel) for each class of signals.
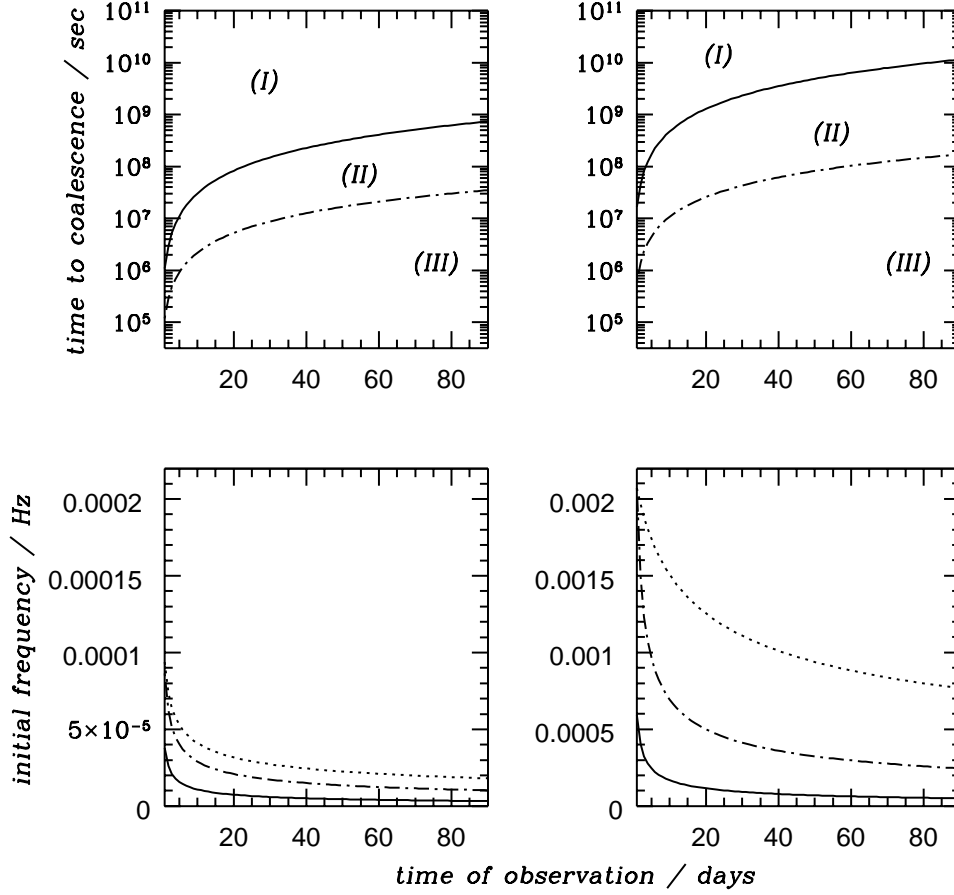
FIG. 2. To show how the partition of signals into different classes depend upon the observation time T_1 we consider two binary systems: $M_1 = M_2 = 10^7 \, M_\odot$ (left panels) and $M_1 = 2 \times 10^6 M_\odot \,, M_2 = 1000 \, M_\odot$ (right panels). The Newtonian time to coalescence τ_n, Eq. (2.23), and the initial frequency f_b, Eq. (2.22), are used to separate the classes: continuous line between I and II, dashed-dotted line between II and III, dotted line between III and IV. The frequency scale has been chosen so that f_{isco} corresponds to the top of the panel.
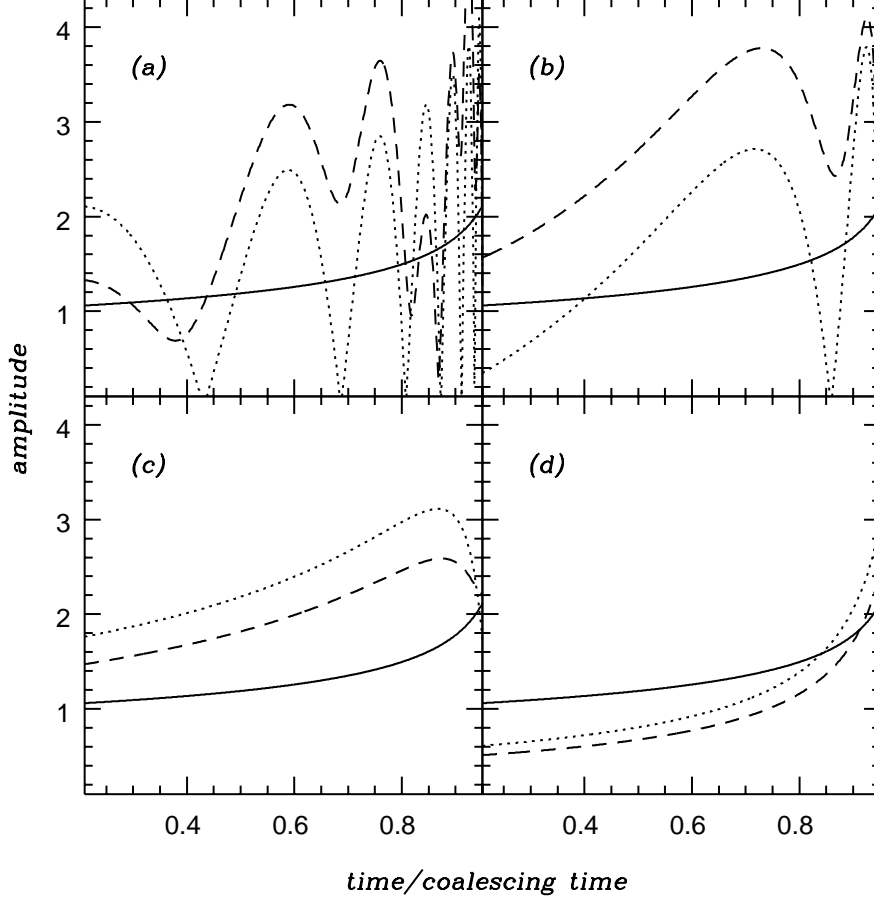
FIG. 3. The effect of the Doppler filter r_θ on in-spiral signals. The plots show a comparison between the chirp amplitude $A(t)$, Eq. (2.5), (solid line) and the Doppler amplitude for different values of the angle θ ($\cos\theta = 0$: dashed-line; $\cos\theta = 0.4$: doted-line) and of the chirp mass: (a) $\mathcal{M} = 10^5\,M_\odot$, (b) $\mathcal{M} = 10^6\,M_\odot$, (c) $\mathcal{M} = 10^7\,M_\odot$, (d) $\mathcal{M} = 10^8\,M_\odot$ ($\eta = 1/4$ for all systems). The chirp amplitudes are normalized to $A(t=0) = 1$; the round-trip light-time is $T = 4000$ sec. Note the increasing modulation induced by the Doppler response as the final merger is approached; this modulation disappears as $\mathcal{M}/T$ increases because the filter degenerates in a multiplicative factor (cfr. Eq. (3.6) and Fig 4).
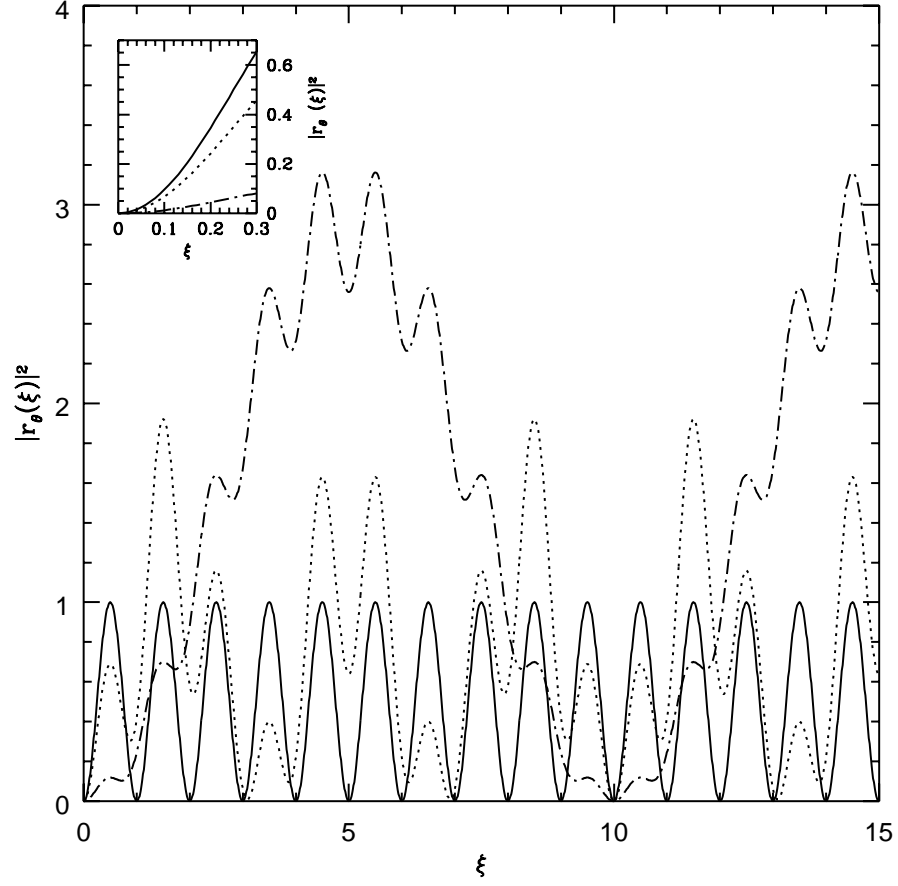
FIG. 4.   The square modulus of the Doppler filter $|\tilde{r}_\theta(\xi)|^2$, Eq. (3.9), as a function of $\xi \equiv f\,T$ for selected values of the angle θ (solid line: $\cos\theta = 0$; dotted-line: $\cos\theta = 0.4$; dotted-dashed line: $\cos\theta = 0.8$). The small box zooms the behavior of $|\tilde{r}_\theta(\xi)|^2$ for $\xi \ll 1$; note that, only when ξ is small, $|\tilde{r}_\theta(\xi)|^2$ is a monotonic decreasing function of $\cos\theta$, which is not true for $\xi \gtrsim 1$.
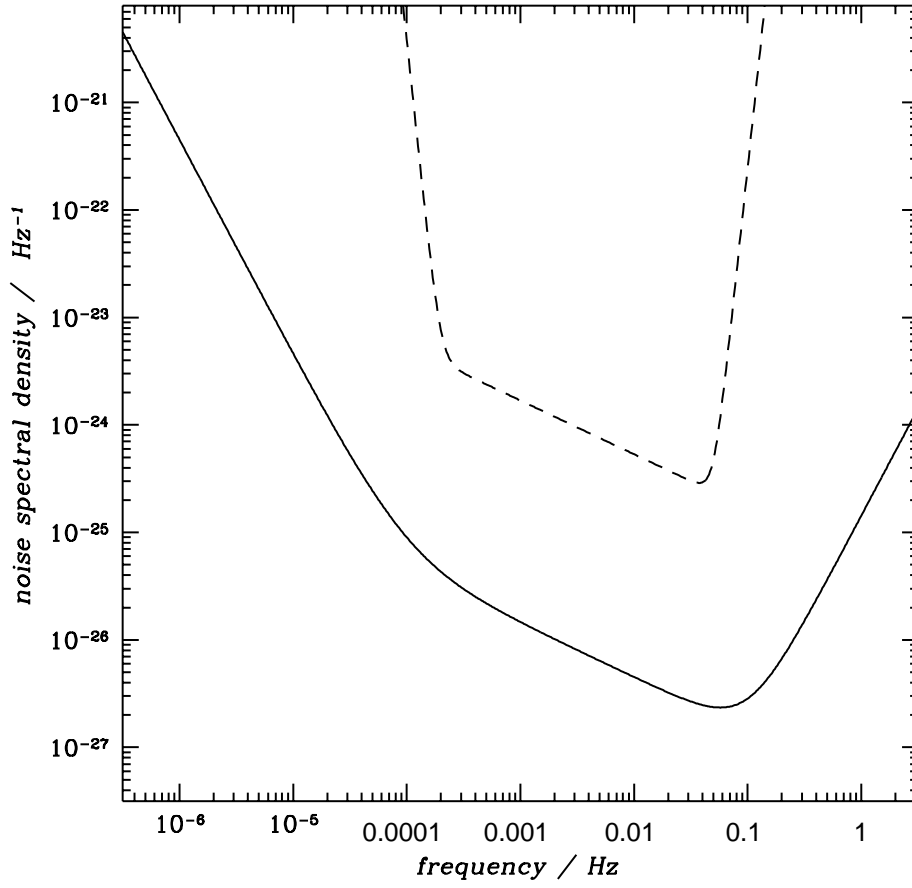
FIG. 5. Noise spectral density of CASSINI (solid line) and ULYSSES (dash-line). $S_n(f)$ is computed according to Eqs. (4.12) – (4.15) and Table II.
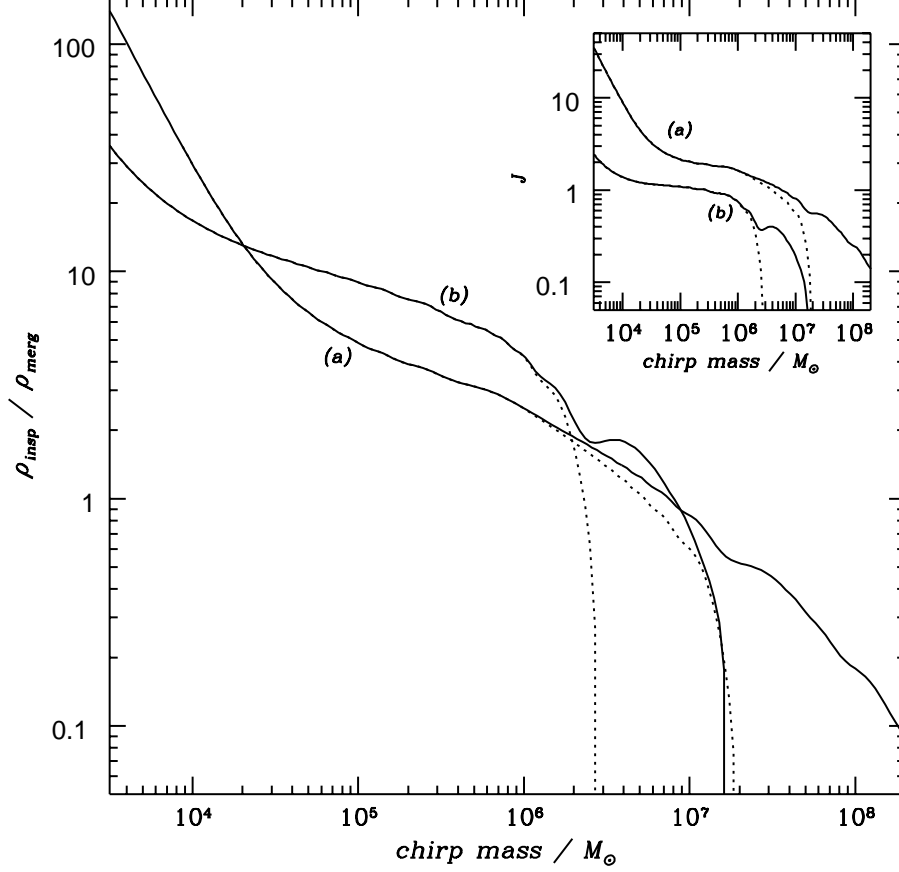
FIG. 6. Comparison of the sensitivity of CASSINI experiments in observations of in-spiral and merger signals. For a given source, the plot shows the ratio of the optimal SNR achievable in observations of the in-spiral signal, ρ_{insp}, with respect to that produced during the merger phase, ρ_{merg}, as a function of the chirp mass and for the mass ratios 1 and 0.01, label (a) and (b) respectively. The solid lines refer to the low frequency cut-off 10^{-6} Hz, whereas the dotted lines to 10^{-4} Hz. The small box shows, for the same cases, the relative overlap J, Eq. (4.26), of the in-spiral and merger signal with respect to the instrument response. The time of observation is assumed to be $T_1 = 40$ days and the noise spectral density $S_n(f)$ is computed according to Eqs. (4.12) – (4.15) and Table II.
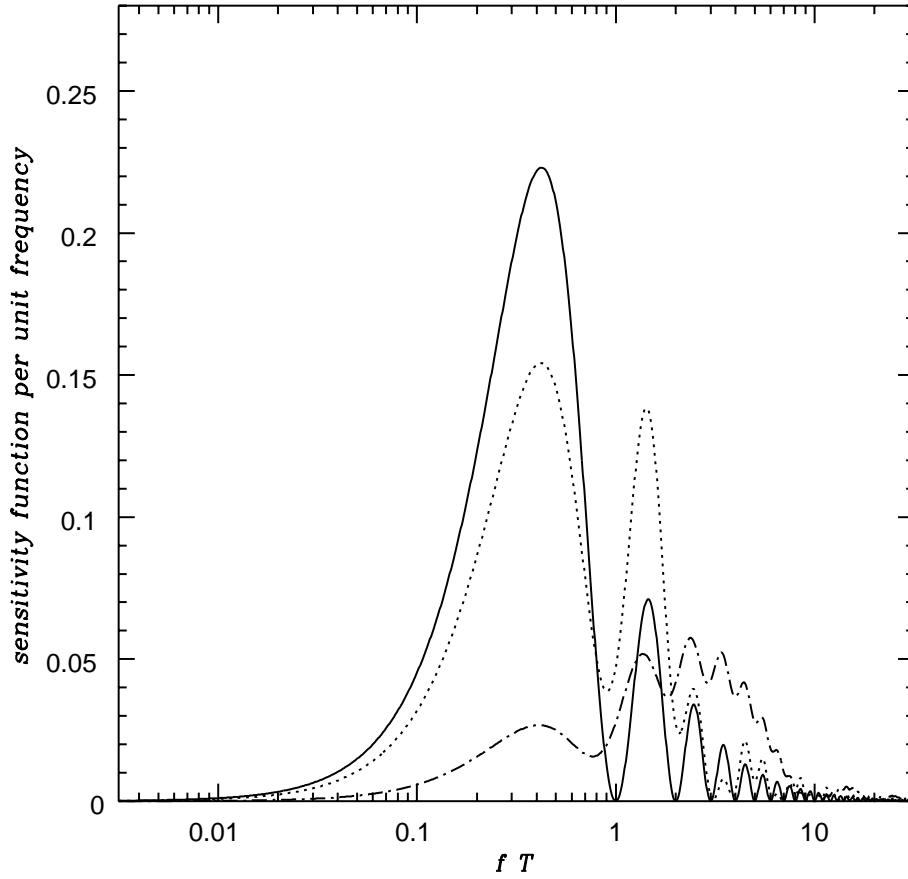
FIG. 7. The spectrum $\tilde{\Upsilon}(f)$ of the sensitivity function, see Eq. (4.17). We have used CASSINI's noise parameters, Table II and Fig. 5 (solid line: $\cos\theta = 0$; dotted line: $\cos\theta = 0.4$; dotted-dashed line: $\cos\theta = 0.8$).
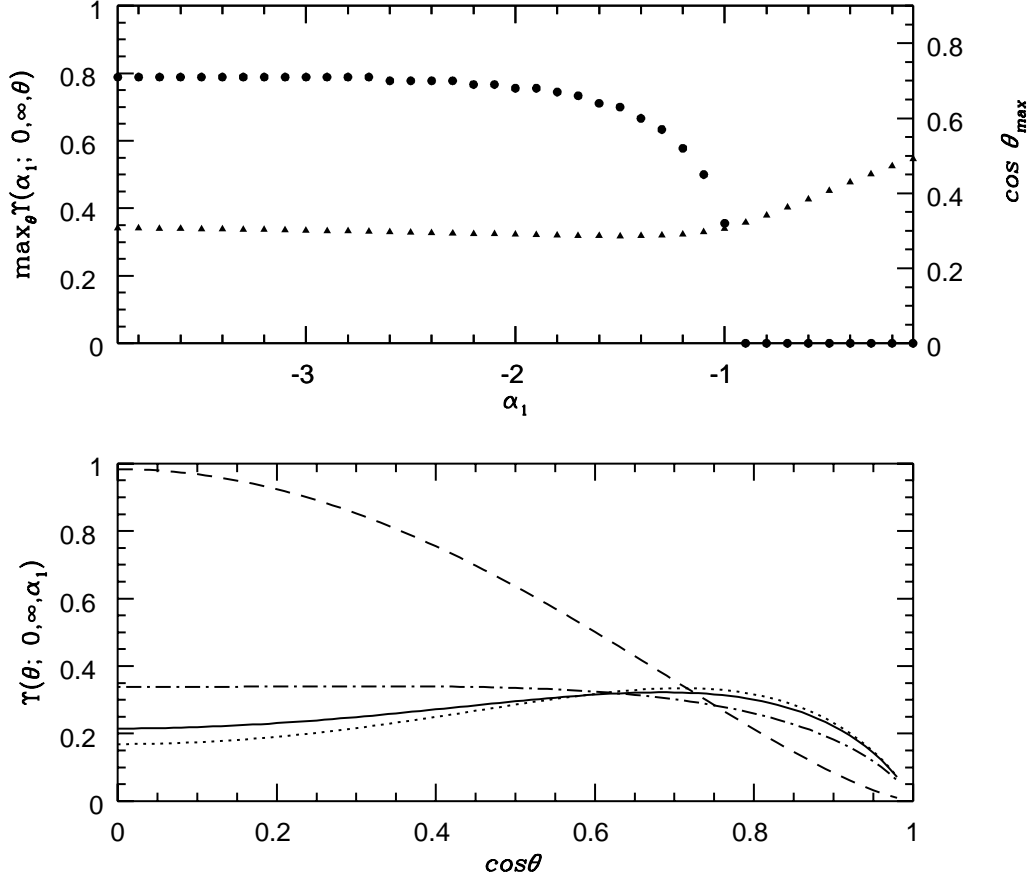
FIG. 8. The deterioration of the sensitivity function Υ, and therefore of the SNR, due to the angle θ between the source and the probe and the redness of the spectrum at low frequencies, given by α_1 (cfr. Eqs. (4.12) – (4.15) and Table II), as described by the function $\Upsilon(\xi_e = 0, \xi_b = \infty, \theta; \alpha_1)$. In the upper panel we show, as a function of α_1, the maximum value of $\Upsilon(\xi_e = 0, \xi_b = \infty, \theta; \alpha_1)$ (triangles) and the angle θ_{max} (bullets) at which it is attained. The 'normal' value $\theta_{max} = \pi/2$ occurs above $\alpha_1 \simeq -0.9$. The lower panel shows the behavior of $\Upsilon(\xi_e = 0, \xi_b = \infty, \theta; \alpha_1)$ as a function of $\cos\theta$ for the case $\alpha_1 = 0$ (dashed line), $\alpha_1 = -1$ (dotted-dashed line), $\alpha_1 = -2$ (continuous line) and $\alpha_1 = -3$ (dotted line); the values of α_2 and α_3 are $-1/2$ and $+2$, respectively, corresponding to those of the CASSINI experiments. Note that, for $\alpha_1 \leq -1$, the smallest deterioration does not occur at the obvious value $\theta = \pi/2$; in particular, for $\alpha_1 = -2$ it occurs at $\cos\theta \simeq 0.68$, so that a small signal enhancement with respect to the ideal case is possible.

41
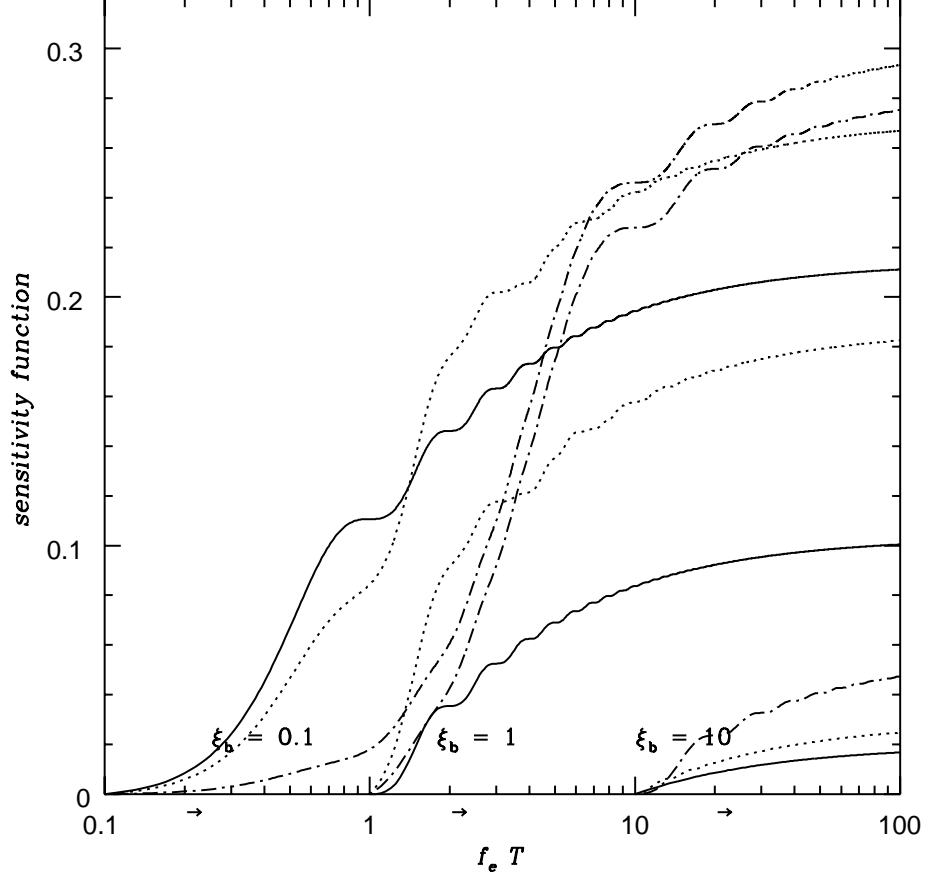
FIG. 9. The behavior of the sensitivity function Υ as a function of the final frequency f_e (in units of the round-trip light-time T) for selected values of the initial frequency $T f_b = \xi_b = 0.1\,,1\,,10$ (see labels). CASSINI's noise parameters have been used (Table II and Fig. 5). To the right of the arrows we have broad band searches with $f_e - f_b > f_b$ (solid line: $\cos\theta = 0$; dotted line: $\cos\theta = 0.4$; dotted-dashed line: $\cos\theta = 0.8$).
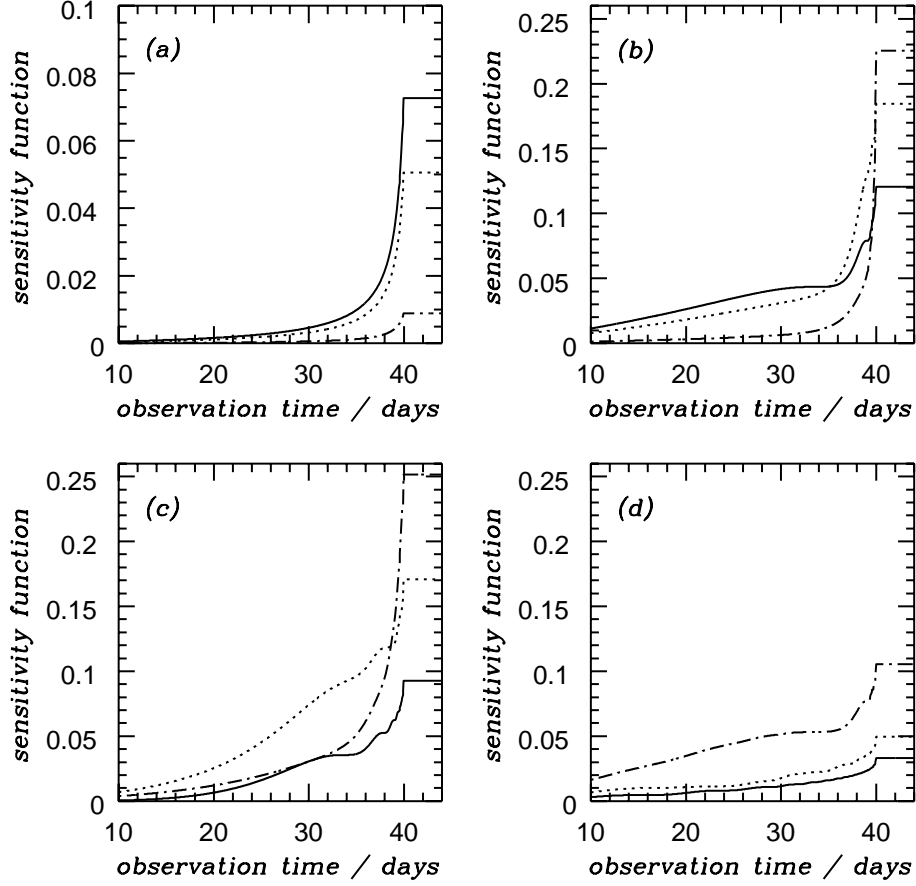
FIG. 10. The behavior of the sensitivity function Υ as a function of T_1, for the four fiducial sources described in the text and in Table III (panels (a) to (d), respectively), with $f_b = 10^{-5}, 5 \times 10^{-5}, 10^{-4}, 5 \times 10^{-4}$ Hz, equal masses, coalescence at the end of the record and chirp mass almost equal to its the critical value for a 40 days run. The deterioration as T_1 decreases reflects the loss of signal-to-noise ratio due to the narrowing of the band-width (solid line: $\cos\theta = 0$; dotted line: $\cos\theta = 0.4$; dotted-dashed line: $\cos\theta = 0.8$). Notice the different scale in panel (a).
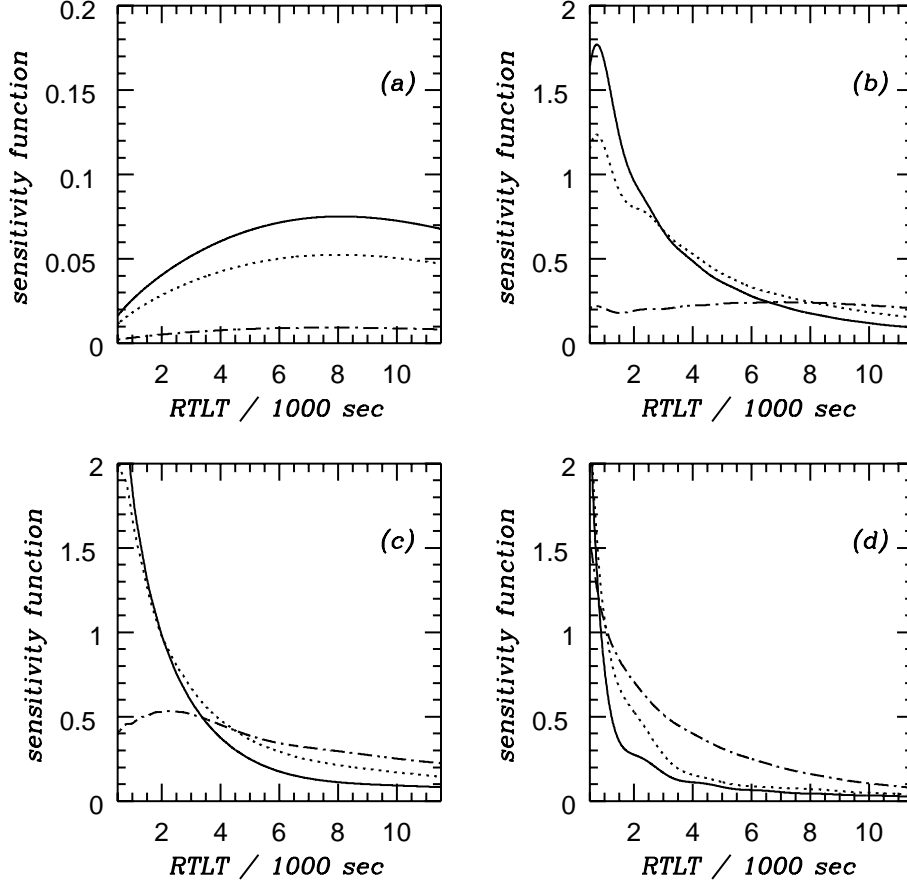
FIG. 11.   The behavior of the sensitivity function Υ as a function of the round-trip light time for same four fiducial sources of the previous Figure (solid line: $\cos\theta = 0$; dotted line: $\cos\theta = 0.4$; dotted-dashed line: $\cos\theta = 0.8$). Notice the different scale in panel (a).
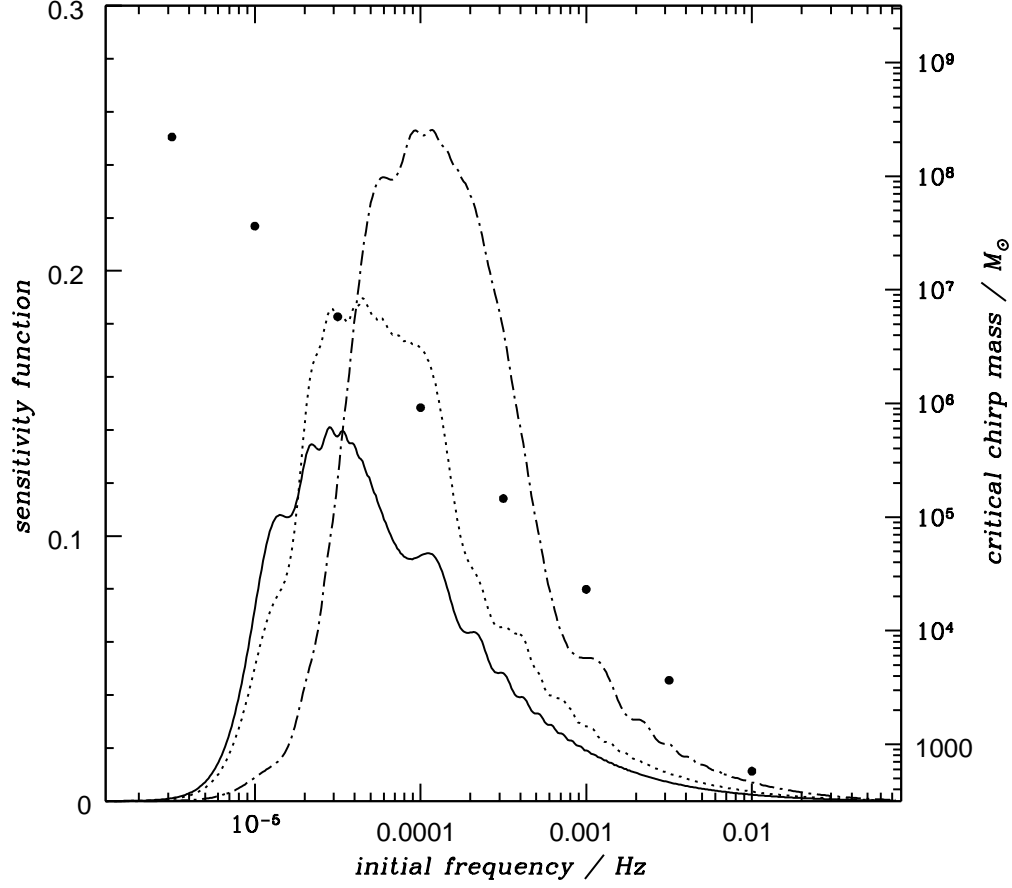
FIG. 12. The behavior of the sensitivity function as a function of the initial frequency f_b for wide band searches of class III, with $f_b = f_B$, $f_e = f_{isco}$ and $T_1 = 40$ days. The corresponding value of the chirp mass – near to the critical value (4.20) – is given by the filled circles (solid line: $\cos\theta = 0$; dotted line: $\cos\theta = 0.4$; dotted-dashed line: $\cos\theta = 0.8$).
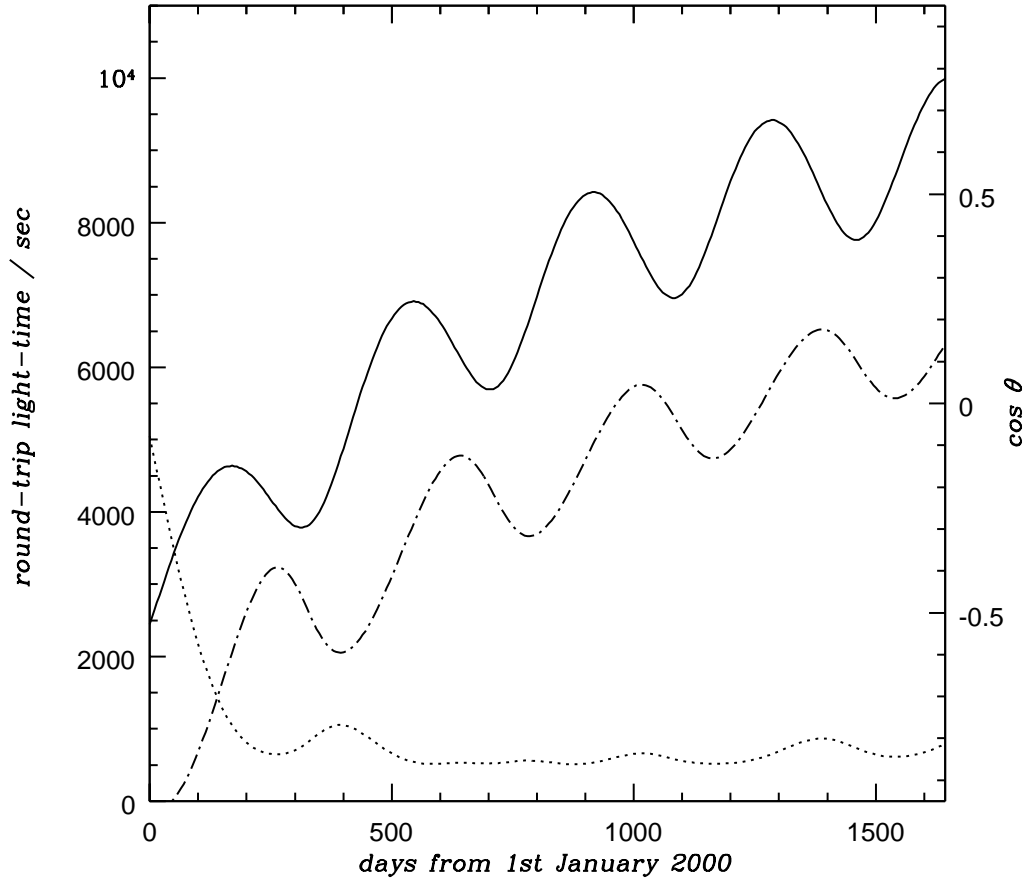
FIG. 13. CASSINI's cruise to Saturn. The solid line gives the round-trip light-time T as function of time and we show also the variation of $\cos\theta$ for the Virgo Cluster (dashed-dotted line) and the Galactic Centre (dotted line). The three gravitational wave experiments take place during the days 695-735, 1071-1111 and 1443-1483 from 1st January 2000.
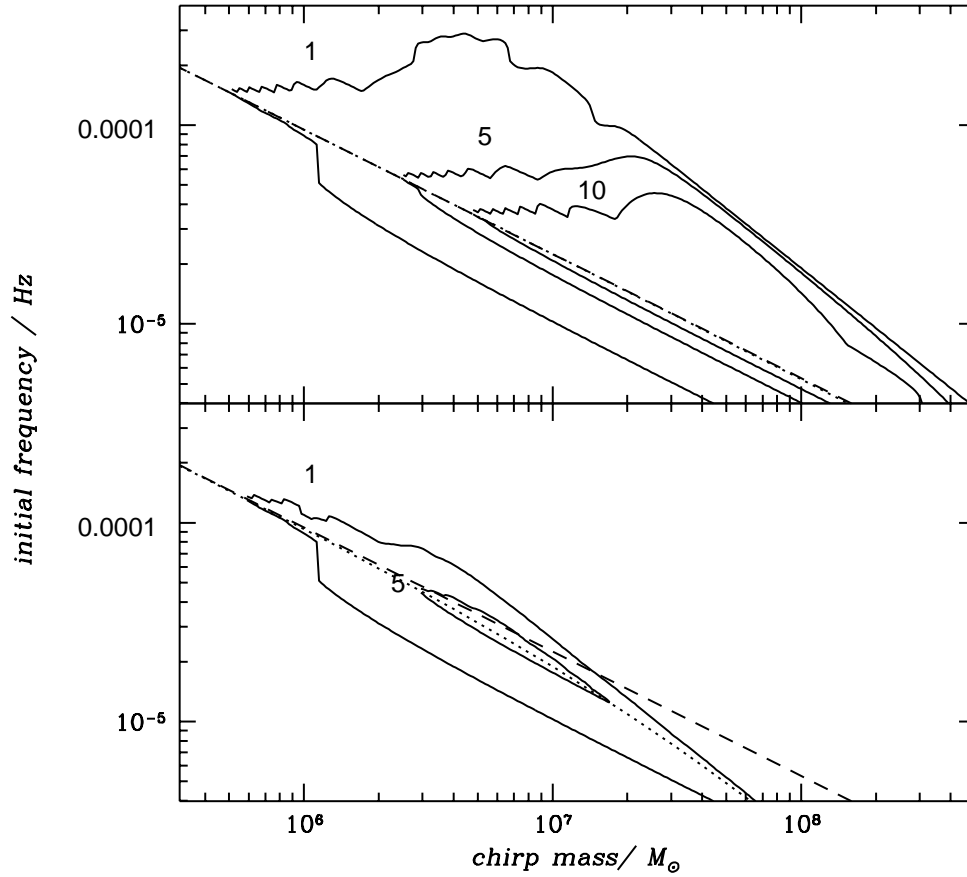
FIG. 14.   Detectable in-spiral signals emitted by binary systems in the Virgo Cluster for the third CASSINI's experiment of 40 days. The contour plots of the SNR (in amplitude) for the levels 1, 5 and 10 are shown. The top and bottom panels refer to the mass ratios $M_2/M_1 = 1$ and 0.01, respectively. In the latter case no signals are observable at $\rho \geq 10$. The dashed diagonal line gives the critical chirp mass $\mathcal{M}_c$, see Eq. (4.20). The dotted line marks the transition between signals of class III and IV. Notice that for $M_1 = M_2$ (upper panel) the two lines almost coincide.
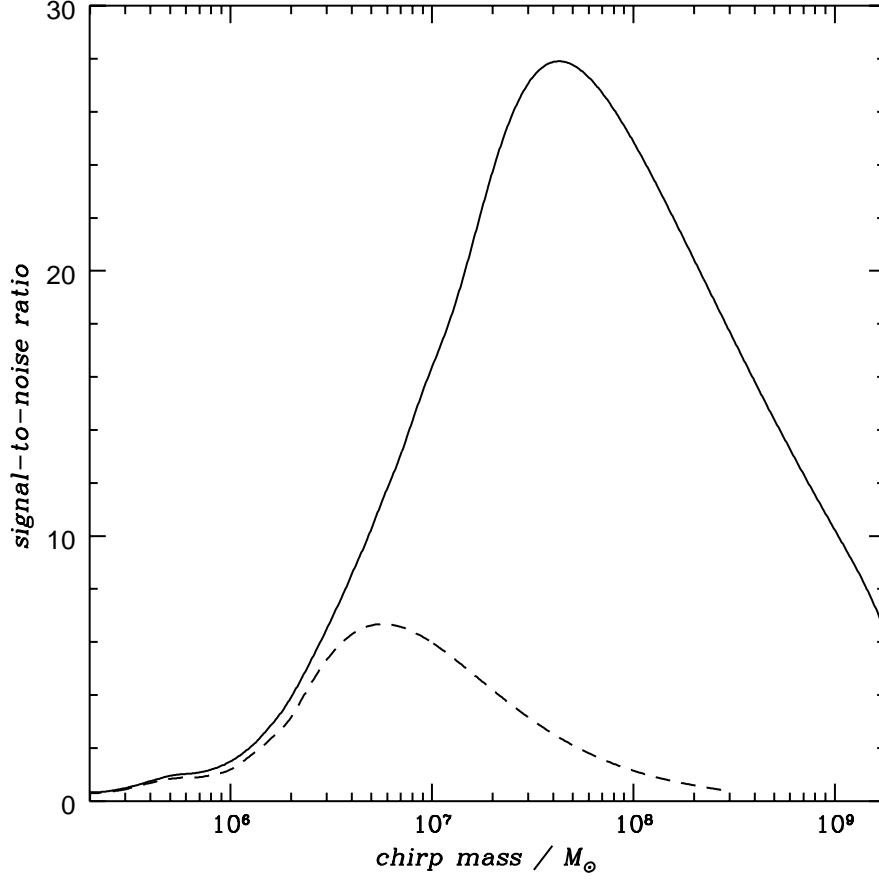
FIG. 15.   Signal-to-noise ratio for in-spiral signals emitted by binaries in the Virgo cluster
(D = 17 Mpc) with coalescence at the end of the record – that is $f_b = f_B$ and $f_e = f_{\mathrm{isco}}$ – as a
function of the chirp mass. The solid line refers to the case $M_1 = M_2$, while the dashed line to
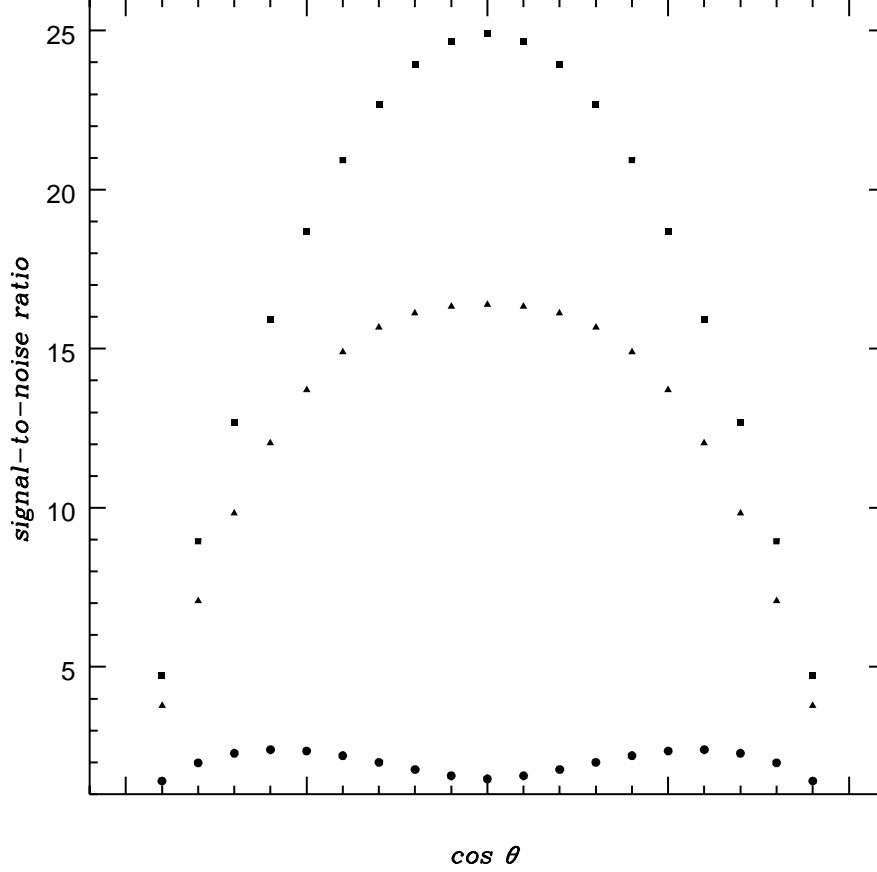$M_2/M_1 = 0.01$. We have considered CASSINI third opposition and $T_1 = 40\,\mathrm{days}$.

FIG. 16. The signal-to-noise ratio as a function of $\cos\theta$ during CASSINI third opposition, $T_1 = 40$ days, for in-spiral signals emitted by binary systems located at the same distance of the Virgo cluster ($D = 17$ Mpc) with $f_b = f_B$ and $f_e = f_{\text{isco}}$, that is final coalescence at the end of the record (squares: $\mathcal{M} = 10^8\,M_\odot$; triangles: $M_\odot = 10^7\,M_\odot$; bullets: $M_\odot = 10^6\,M_\odot$; for all $\eta = 1/4$). The decrease for $|\cos\theta| \to 1$ is of course due to the approach to the case of propagation along the instrument's beam; the saddle in correspondence of $|\cos\theta| \simeq 0$ for $\mathcal{M} = 10^6\,M_\odot$ is due to the fact that the frequency band swept by the signal encounters a minimum of the response function at $fT \approx 1$, which vanishes for $\cos\theta = 0$, see Figs. 4 and 7.
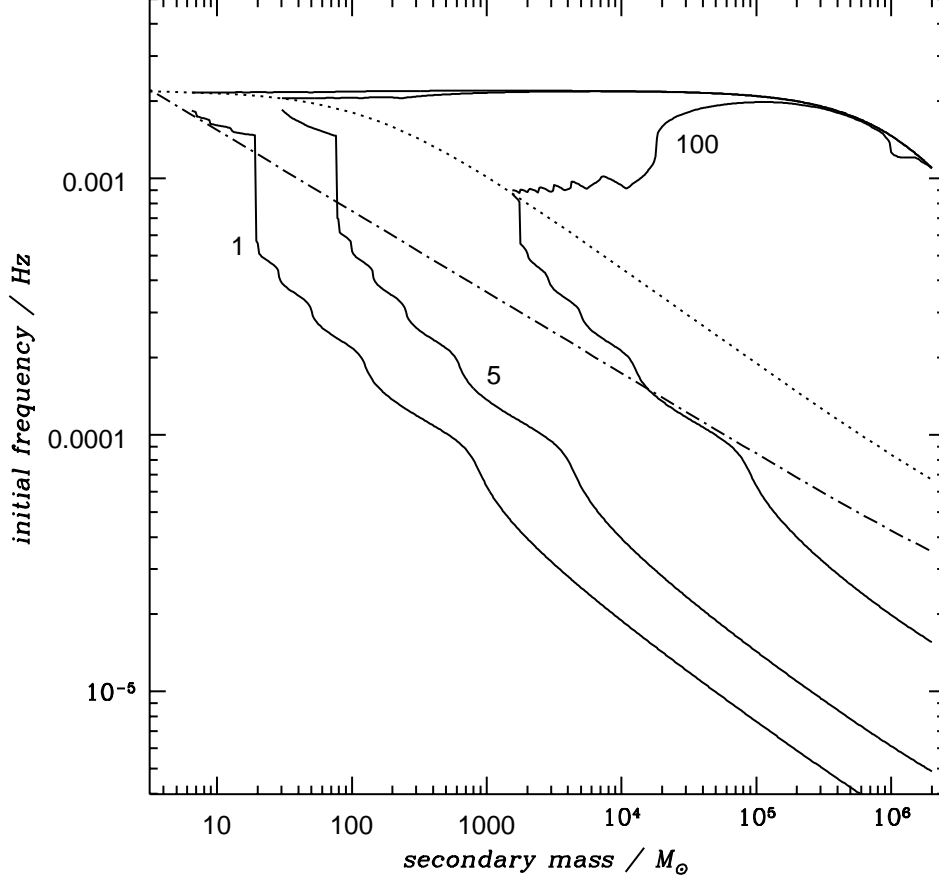
FIG. 17. Detectability of radiation emitted by the in-spiral of a secondary black hole of mass M_2 orbiting a primary object with mass $M_1 = 2 \times 10^6 \, M_\odot$, in the Galactic Centre ($D \simeq 8$ Kpc) during CASSINI's third experiment ($T_1 = 40$ days). The contour plots of SNR $= 1, 5$ and 100 in the plane (M_2, f_b) are shown. The dashed-dotted line divides the plane (M_2, f_b) in signal of class II (below) and III (above), while above the dotted line the signals are registered as of class IV.
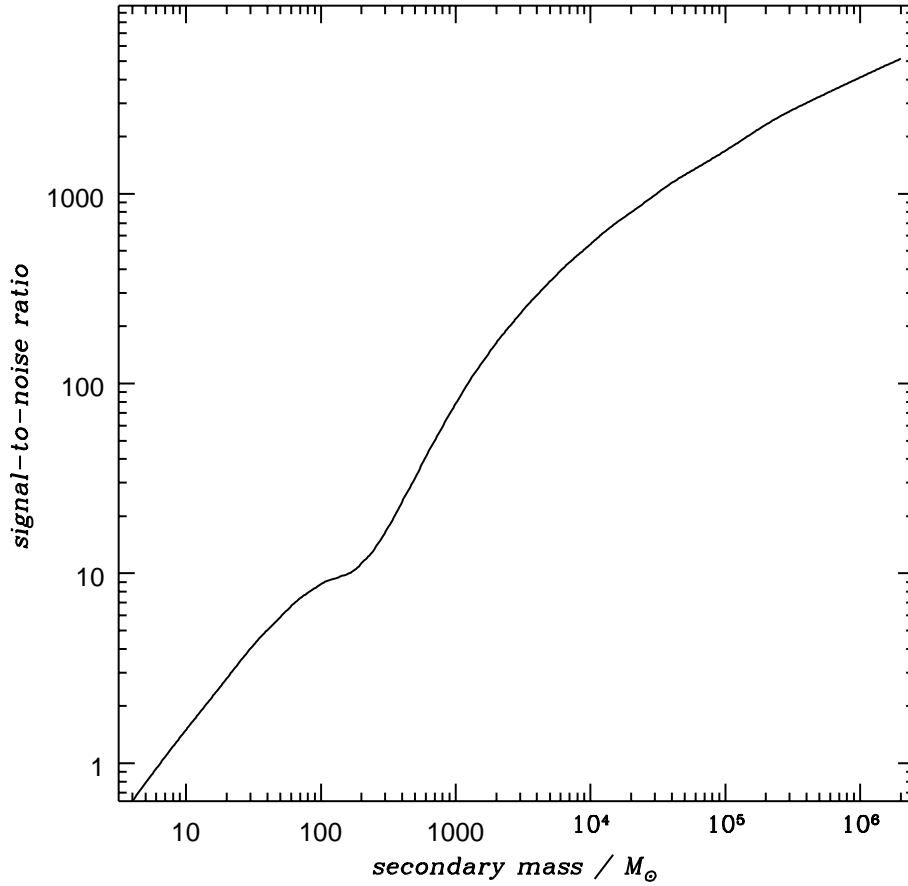
FIG. 18. Expected optimal signal-to-noise ratio produced in CASSINI records by in-spiraling binaries in the Galactic Centre. The plot shows the maximum SNR – *i.e.* computed for $f_b = f_B$ and coalescence at the end of the record ($T_1 = 40$ days), therefore $f_e = f_{\rm isco}$ – produced by binary systems with $M_1 = 2 \times 10^6 \, M_\odot$ and a secondary black hole of mass $M_2 \leq M_1$ as a function of M_2, during CASSINI's third opposition.
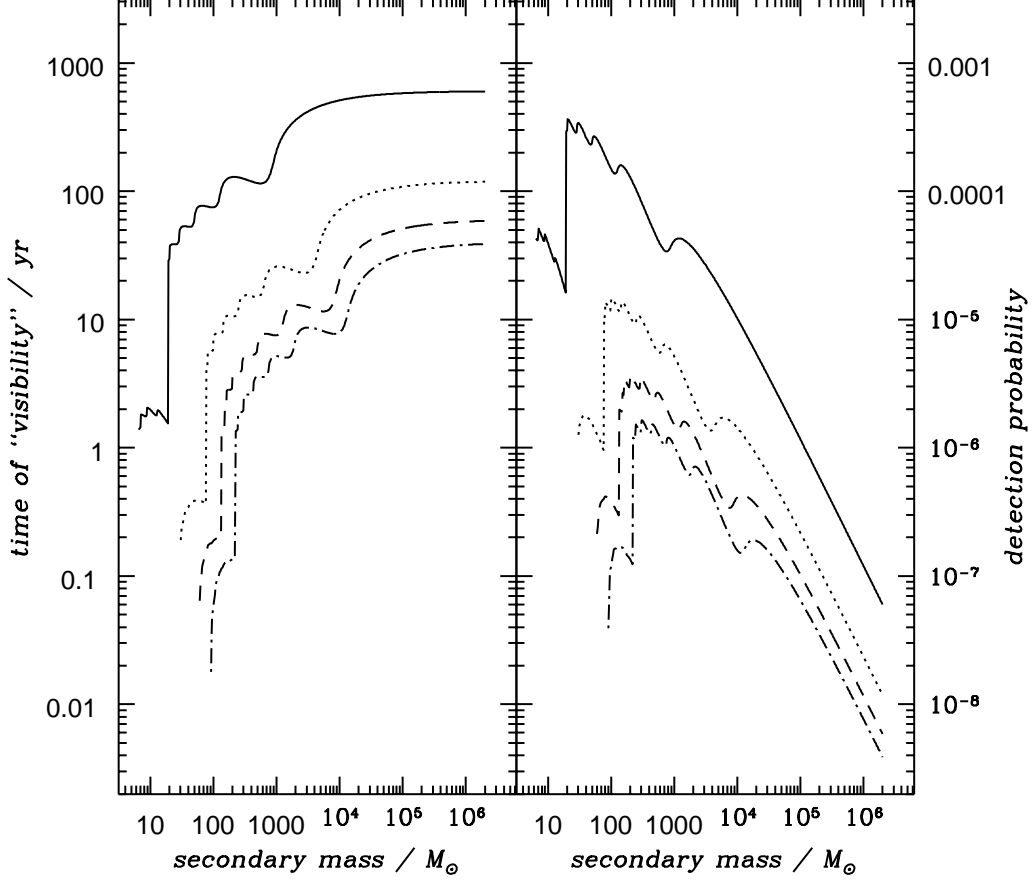
FIG. 19. Time of 'visibility' T_D and probability of success for the detection of radiation emitted by the in-spiral of a secondary black hole into a primary of mass $M_1 = 2 \times 10^6 \, M_\odot$ in Our Galactic Centre during CASSINI third opposition. The curves refer to four different thresholds of detection ($\rho_D = 1$: solid line; $\rho_D = 5$: dotted line; $\rho_D = 10$: dashed line; $\rho_D = 15$: dotted-dashed line).